

Reports from Research Areas

Highly textured Nickel-Tungsten substrate for YBCO coated conductors (graphically altered EBSD image)

Visualization of the spin polaron in LaCoO_3

Iron filled carbon nanotube attached to a conventional AFM cantilever

Unit cell of $\text{Al}_3\text{Li}_4(\text{BH}_4)_{13}$

Research Area 1

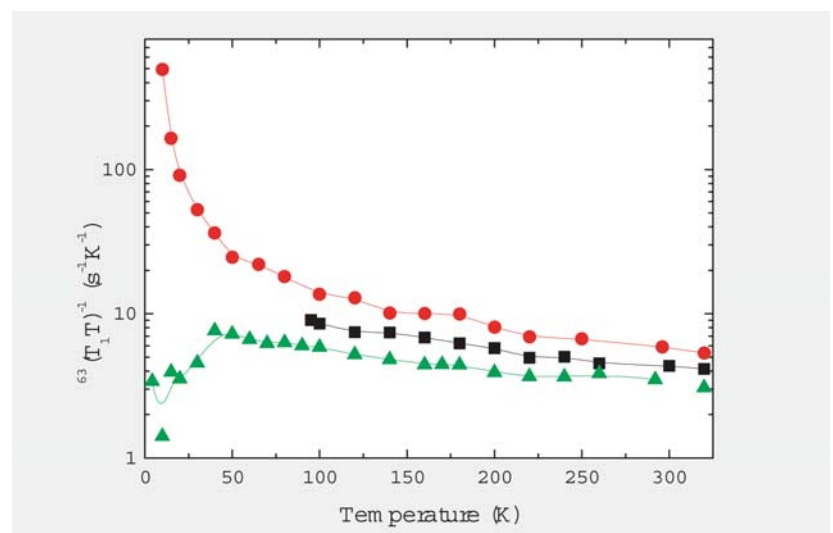
Superconductivity and superconductors

Cu NQR Evidence for a Different Effect of Zn and Ni Doping on the Pseudogap in $(\text{Eu,Nd})\text{Ba}_2(\text{Cu,Zn,Ni})_3\text{O}_7$

H.-J. Grafe, F. Hammerath, T. Wolf¹, G. Khaliullin², V. Kataev, B. Büchner

The origin of the pseudogap in the cuprates and its relation to high temperature (high- T_c) superconductivity is still under debate. Theoretically, it has been related either to a precursor superconducting state without macroscopic phase coherence or to a kind of order that may even compete with superconductivity such as a stripe order or spin and charge density waves. Experimentally, measurements of the optical conductivity [1] that probe the *charge* excitations in $(\text{Eu,Nd})\text{Ba}_2(\text{Cu,Zn,Ni})_3\text{O}_7$ show that large Zn impurity doping suppresses the charge pseudogap, whereas large amounts of Ni enhances its energy scale. Therefore we have investigated the *spin* dynamics by means of nuclear quadrupole resonance (NQR) measurements on the Cu nucleus in these compounds [2]. Whereas our previous measurements were somewhat affected by the additional magnetic moment of the Nd, we could now measure single crystals of $\text{EuBa}_2(\text{Cu,Zn,Ni})_3\text{O}_7$ where the Eu is non-magnetic [3]. We find that Ni doping enhances the nuclear spin lattice relaxation rate, $(T_1T)^{-1}$, leading to a Curie Weiss like temperature dependence (see Fig.). In contrast, large amounts of Zn reduces $(T_1T)^{-1}$. At low temperatures, this effect is even more pronounced, and the opening of a spin pseudogap in the Zn doped samples is clearly visible. Since $(T_1T)^{-1}$ probes the low frequency dynamic spin susceptibility of the CuO_2 planes at the antiferromagnetic wave vector, \mathbf{Q}_{af} , we conclude that Ni enhances antiferromagnetic correlations, and thereby the hole localization and the charge pseudogap. In contrast, large amounts of Zn dilute the spin system, and thus the low energy spin collective modes are suppressed, resulting in a (spin) pseudogap like decrease of $(T_1T)^{-1}$ at low temperatures. Our results reveal hence an intimate relationship between magnetic correlations and the charge pseudogap phenomenon in high- T_c cuprates.

Fig.: Cu spin lattice relaxation rate divided by temperature, $(T_1T)^{-1}$, for undoped (black squares), Zn doped (green triangles) and Ni doped (red dots) $\text{EuBa}_2(\text{Cu,Zn,Ni})_3\text{O}_7$. Ni doping enhances $(T_1T)^{-1}$, while Zn doping reduces $(T_1T)^{-1}$ leading to a pseudogap like decrease below ~ 40 K.



[1] A. V. Pimenov *et al.*, Phys. Rev. Lett. **94**, 227003 (2005)

[2] H.-J. Grafe *et al.*, Phys. Rev. B **77**, 014522 (2008)

[3] H.-J. Grafe *et al.*, preprint

Cooperation ¹Forschungszentrum Karlsruhe, Germany; ²Max-Planck-Institut für Festkörperforschung, Stuttgart, Germany

Funded by DFG, Forschergruppe 538

YBCO coated conductor architectures

B. Holzapfel, R. Hühne, J. Eickemeyer, U. Gaitzsch, A. Güth, C. Rodig, H. Klauß, J. Freudenberger, J. Hänisch, M. Sparing, B. Rellinghaus, R. Gärtner, T. Thersleff, A. Kirchner, T. Freudenberg, M. Erbe, M. Schubert, L. Schultz

The preparation of coated conductor architectures for high-performance superconducting tapes based on YBCO films was continued last year in the framework of an IFW project. A major part of the work was dedicated to the development of improved textured metal substrates showing a reduced ferromagnetism at 77 K and higher mechanical strength compared to the standard Ni-5at%W tape. For the first time, highly textured Ni-9at%W tapes were realized using specific homogenisation and stress relief treatments leading to a cube orientated fraction of more than 94 % [1]. Simultaneously, the preparation of Ni-7.5at%W substrates was optimised resulting in an improved texture with a cube orientated fraction of more than 97 %. A standard $\text{Y}_2\text{O}_3/\text{YSZ}/\text{CeO}_2$ coated conductor architecture was prepared on these substrates using pulsed laser deposition. The final YBCO layers showed an in-plane alignment below 8° and a critical current density of 1.1 MA/cm^2 on Ni-9at%W and 1.25 MA/cm^2 on Ni-7.5at%W, respectively (see Fig.).

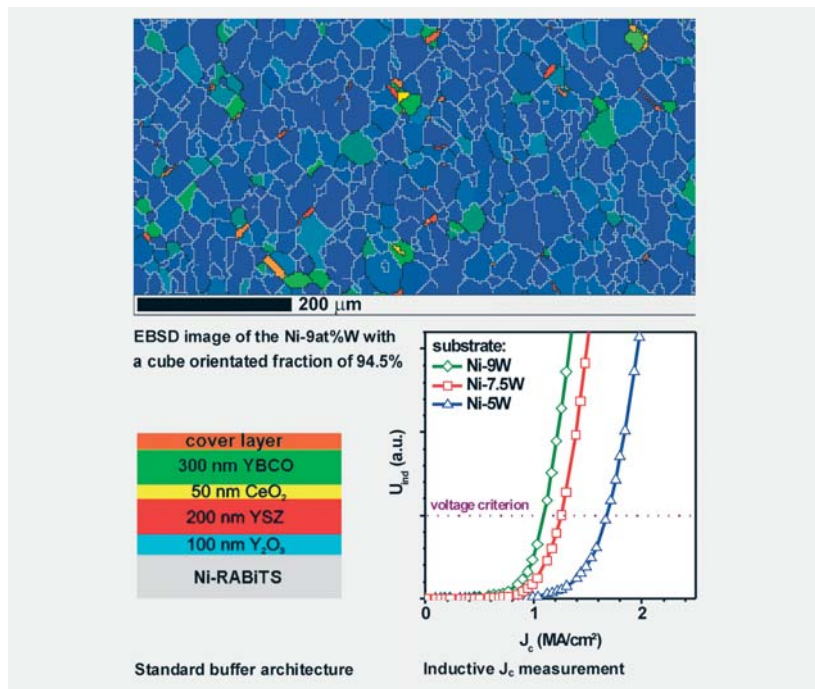


Fig.: Newly developed highly textured Ni-9at%W substrates as templates for YBCO coated conductors [1].

Furthermore, the work was focused on the improvement of the critical current density of the superconducting layer in magnetic fields by the incorporation of artificial pinning centres. Pulsed laser deposition as well as chemical solution deposition was used to implement different second phase materials, as for example $\text{Y}_2\text{Ba}_4\text{Cu}(\text{Nb,Zr})\text{O}_y$ [2], BaZrO_3 or BaHfO_3 in the YBCO matrix. The influence of these nanoparticles on the local structure of the grown film was investigated in detail using high resolution transmission electron microscopy in order to correlate the defect structures to the measured electrical properties of the YBCO layer. As a result, it was found that the J_c anisotropy of the superconducting layer can be tuned by adapting deposition parameters like temperature or deposition rate.

[1] R. Hühne et al., Supercond. Sci. Technol. 23 (2010) accepted.

[2] E. Reich et al., Supercond. Sci. Technol. 22 (2009) 105004.

Cooperation evico GmbH, Univ. Cambridge, Gent Univ., Zenergy GmbH, ICMA Barcelona, Shanghai Univ., Bruker HTS GmbH

Funded by BMBF, EU, DAAD

Plasmon Dispersion vs. Charge Order in Transition-Metal Dichalcogenides?

R. Schuster, M. Knupfer, B. Büchner

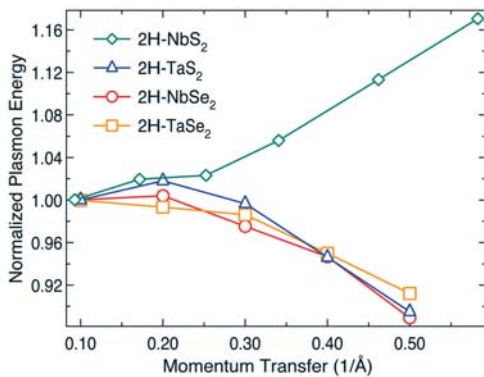


Fig.: Dispersion of the charge carrier plasmon for different representatives of the transition-metal dichalcogenides measured at room temperature. The curves are normalized to their onset values at 0.1\AA^{-1} .

The transition-metal dichalcogenides are quasi-2D metallic systems that are known to exhibit different electronic instabilities as a function of temperature. Prominent representatives are $2H\text{-TaSe}_2$, $2H\text{-TaS}_2$ and $2H\text{-NbSe}_2$ all undergoing a charge-density wave (CDW) transition followed by the onset of superconductivity at lower temperatures. Another very similar member of this class is $2H\text{-NbS}_2$ which, however, does not show any signs of charge order. In addition to the above mentioned phase transitions, the conduction electrons, derived mainly from the transition-metal ions, can also perform collective density oscillations – so called plasmons – that can be probed with the help of electron energy-loss spectroscopy. Such experiments have been done on $2H\text{-NbS}_2$ in the past and revealed conventional quadratic plasmon dispersion with a positive slope that is theoretically predicted for ordinary metals. We performed similar investigations on the other three above given members of the family and found a remarkably different behavior that is summarized in the figure. All the compounds which are known to undergo the CDW transition show a negative dispersion of the plasmon which contradicts not only the behaviour found in $2H\text{-NbS}_2$ but also the prediction of a positive dispersion for conventional metallic systems. This behavior points to a possible – yet unknown – interference between the plasmon and the CDW. But even if the coexistence of negative plasmon dispersion and the charge order is purely accidental the negative dispersion poses considerable theoretical questions.

Cooperation Institut de Physique de la Matière Complexe, Ecole Polytechnique Fédérale de Lausanne, Switzerland

Funded by DFG

MgB₂ – Preparation of first 1000 m long multifilamentary wire

M. Herrmann, W. Häßler, A. Kario, C. Rodig, D. Seifert, T. Wolf, H.-P. Trink, J. Scheiter, M. Schubert, K. Nenkov, G. Fuchs, B. Holzapfel, L. Schultz



Fig.: First 1000 m multifilamentary MgB₂ wire using mechanically alloyed in-situ powder manufactured under industrial production conditions

The collaboration with Bruker HTS succeeded in the preparation of a single piece multifilamentary wire exceeding a 1000 m in length with a J_c of up to 91 A/mm^2 at 4.2 K and 5 T. This conductor, using a mechanically alloyed in-situ MgB₂ precursor prepared at IFW was manufactured under industrial production conditions at Bruker HTS. Only a reasonable interplay of both key parameters, an appropriate preparation route and high current carrying capability, will allow for a widespread use of MgB₂ conductors.

Detailed studies on the influence of the milling parameters, e.g. time and speed of processing has been done and showed, that the morphology of the powder is strongly affected. With increasing milling energy, a refined particle size down to several nanometer, improved homogeneity of the powder and subsequently improved critical current densities in the wires are observed. At the same time the decreasing flowability of the precursor changes the deformability of the conductor when used in the powder-in-tube approach. In order to allow for an easy and reliable production of MgB₂ wires on the kilometer scale, it was essential to prepare a precursor which could be deformed properly within the sophisticated architecture of the conductor as required for all different aspects of the application.

Cooperation Bruker HTS GmbH Alzenau, Slovak Academy of Science - Institute of Electrical Engineering Bratislava, Karlsruhe Institute of Technology

Funded by EAS Bruker GmbH, DAAD, NESPA

Research Area 2

Magnetism and magnetic materials

Hole induced spin polarons in LaCoO₃

A. Alfonsov, E. Vavilova¹, A. Podlesnyak², D.I. Khomskii³, V. Kataev, B. Büchner

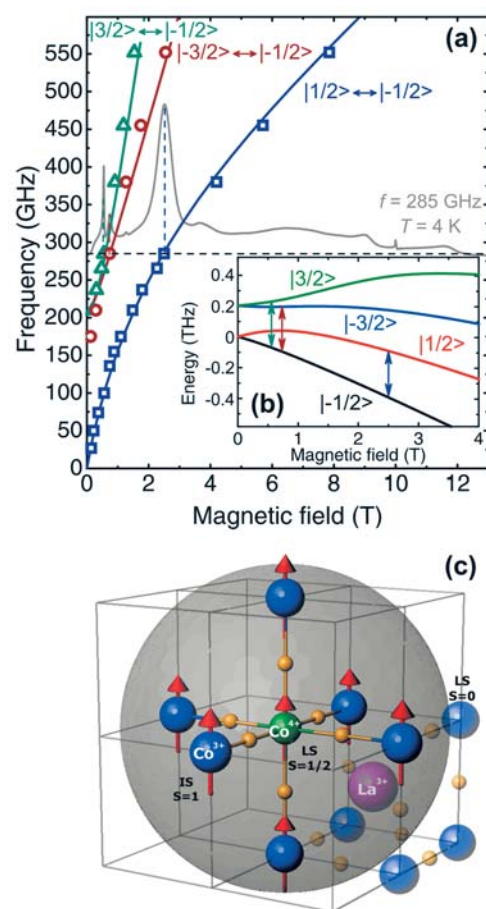
LaCoO₃ is nonmagnetic at low temperatures and shows a temperature activated magnetism due to a change of the Co³⁺ spin state. Surprisingly, a very small hole doping (<0.5 %) via Sr²⁺ or Ca²⁺ substitution for La³⁺ yields a strong magnetization already at low temperatures. The expected saturation magnetic moment should not exceed 5 μ_B per doped hole, which is the maximum possible value for the Co ion transformed into the 4+ oxidation state due to the heterovalent Sr/Ca substitution at the La site. In fact, the magnetic field dependence of the magnetization yields a much higher value of $\sim 15 \mu_B/\text{hole}$. To uncover the nature of this effect we have measured electron spin resonance (ESR) on La_{0.998}Sr_{0.002}CoO₃ and La_{0.998}Ca_{0.002}CoO₃ samples using the unique possibilities of the high field ESR laboratory at the IFW Dresden. The home made setup enables high sensitive measurements in the frequency range from 10 GHz to 1 THz, in the magnetic fields up to 17 T and at temperatures from 300 K down to 2 K. The low temperature ESR experiments reveal multiple resonance excitations indicating the occurrence of extended clusters (spin polarons) with a high spin value and substantial orbital contribution to the magnetism (Fig.). We have found out that the crucial role in the formation of the spin polaron is played by the introduced hole: It turns the oxidation state of the central Co ion to 4+, changes the spin states of 6 neighbouring Co³⁺ ions and couples them ferromagnetically through the double exchange mechanism (Fig.). Details of the ESR experiments, supporting nuclear magnetic resonance and inelastic neutron scattering measurements, as well as the discussion of the spin polaron model can be found in Ref. [1].

[1] A. Podlesnyak et al., Phys. Rev. Lett. 101, 247603 (2008)

Fig. a) The ESR spectrum measured at a frequency $f = 285$ GHz and a temperature $T = 4$ K (gray line); the frequency dependence of the three most intense resonance lines at $T = 4$ K (cyan triangles, brown circles and blue squares). Solid lines (cyan, brown and blue) represent a calculated frequency dependence of the ESR absorption lines of the spin polaron with the spin $S = 13/2$, g -factor of ~ 2.6 and the anisotropy energy gap of ~ 100 GHz (~ 0.4 meV).

b) Calculated energy levels diagram of the spin polaron with $S = 13/2$ (high energy S_z states $|\pm 5/2\rangle$ to $|\pm 13/2\rangle$ are not shown). Arrows represent the three most intense ESR transitions between the S_z states $|3/2\rangle \leftrightarrow |-1/2\rangle$, $|-3/2\rangle \leftrightarrow |-1/2\rangle$ and $|1/2\rangle \leftrightarrow |-1/2\rangle$ at a frequency $f = 285$ GHz and a temperature $T = 4$ K [see panel (a)].

c) Visualization of the spin polaron in LaCoO₃. A central Co⁴⁺ ion in the low spin (LS) $S = 1/2$ state is surrounded by 6 Co³⁺ ions in the intermediate spin (IS) $S = 1$ state. The hole is dynamically distributed over the cluster providing a ferromagnetic coupling of spins via the double-exchange mechanism.



Cooperations ¹Zavoisky Physical Technical Institute, RAS, Kazan, Russia; ²Oak Ridge National Laboratory, Oak Ridge, USA; ³II. Physikalisches Institut, Universität zu Köln, Köln, Germany

Funded by DFG, IMPRS

LSDA+U revisited

K. Koepnik, W. E. Pickett¹, E. R. Ylvisaker¹

Density functional theory (DFT) is an amazingly successful tool to quantitatively describe many properties of solids, surfaces and molecules in the limit of “weak” correlation. In its practical implementation DFT is based on the local spin density approximation (LSDA) or gradient corrected schemes (GGA), which includes the full correlation

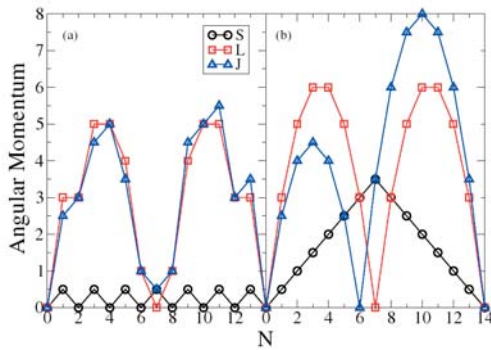


Fig.: Spin (S), orbital (L) and total (J) angular momentum for an isolated 4f-shell as a function of the total 4f-shell occupation. The left panel shows the results for the AMF functional and clearly violates Hund's first rule, while the right panel (AL/FLL functional) follows Hund's rules.

energy of the homogeneous electron liquid. This approach is lacking effects of the energy dependence of the electronic self-energy and contains spurious self-interactions, which becomes important in strongly correlated systems. One commonly used simplistic remedy for these problems is the LSDA+U scheme, which incorporates an ad-hoc occupation number dependent term to the functional. There are many heuristic arguments involved in its construction and consequently several different flavors of the theory exist. We investigated the physical implications of the various flavors of LSDA+U, based both on a theoretical analysis and on numerical calculations. It turns out that among the two commonly used flavors one exhibits a very strange behavior with respect to predicted ground state properties, which leads to a violation of Hund's first rule for isolated atoms. Our analytical results increase the understanding of the physical effects of these kinds of functionals and may lead to improved functionals. It is conceivable that this kind of discussion will also have implications for the LSDA+dynamical mean-field (DMFT) theory, since it is based on a similar ad-hoc Hamiltonian.

Cooperation ¹Univ. of California Davis, USA

Angle-resolved Photoemission Spectroscopy of Spin – Ladder Compounds

A. Koitzsch, D. S. Inosov¹, H. Shiozawa², V. B. Zabolotnyy, S. V. Borisenko, A. Varykhalov³, C. Hess, M. Knupfer, U. Ammerahl⁴, A. Revcolevschi⁴, and B. Büchner

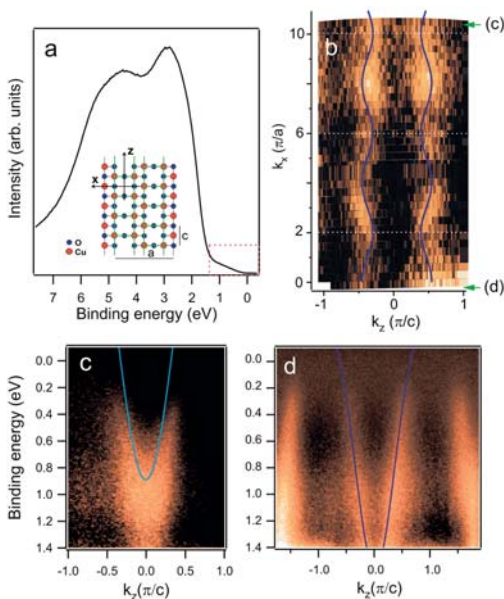


Fig.: Photoemission spectra of $\text{Sr}_{14}\text{Cu}_{24}\text{O}_{41}$. (a) k -integrated valence band. Inset: Crystal structure of the ladder plane. (b) Map of photoemission intensity at $E_B = 0.4$ eV integrated over $\Delta E = 0.08$ eV. The blue line corresponds to the tight binding fit of bandstructure calculations for the bonding band [5]. Green arrows mark the k_x positions of the measurements in (c+d). (c) Intensity map with perpendicular polarization. The light blue line corresponds to the antibonding band of [5]. (d) Intensity map taken with parallel polarization.

One of the peculiar properties of the cuprates is their ability to form sophisticated crystal structures where copper-oxygen networks with a dimensionality between one and two can occur – so called ladder compounds. Cuprate two-leg ladder compounds of the type $\text{Sr}_{14-x}\text{Ca}_x\text{Cu}_{24}\text{O}_{41}$ have been in the focus of intense research for many reasons: i) they are believed to be relevant for the cuprate high- T_c problem, both as simpler paradigm of t - J models [1] and due to the known affinity of the two-dimensional cuprates to one-dimensional (stripe) phenomena [2], ii) as quasi one-dimensional materials they are subject to strong quantum fluctuations and complex density wave order, giving rise to exotic ground states [3], iii) they are superconductors in their own right with an unresolved pairing mechanism [4]. We have investigated the electronic structure of $\text{Sr}_{14-x}\text{Ca}_x\text{Cu}_{24}\text{O}_{41}$ ($x = 0; 11.5$) single crystals by angle-resolved photoemission spectroscopy. Remarkable agreement with bandstructure calculations is found. The Fermi surface is observed for $\text{Sr}_{2.5}\text{Ca}_{11.5}\text{Cu}_{24}\text{O}_{41}$ from which we derive a charge carrier concentration between 0.15 and 0.2 holes per Cu atom at $T = 25$ K in the ladder substructure. The chain substructures, on the other hand, act as diffraction grating for the ladder photoelectrons giving rise to incommensurate replicas of the ladder bands. A low energy band renormalization, a kink, is observed at $E = 70$ meV for $\text{Sr}_{2.5}\text{Ca}_{11.5}\text{Cu}_{24}\text{O}_{41}$. The kink is similar to the one found in two-dimensional cuprates, suggesting a close relationship between the latter and ladder compounds with high internal pressure.

- [1] E. Dagotto et al., *Phys. Rev. B* **45**, 5744 (1992)
- [2] J. M. Tranquada et al., *Nature* **375**, 561 (1995)
- [3] T. Vuletic et al., *Phys. Rep.* **428**, 169 (2006)
- [4] M. Uehara et al., *J. Phys. Soc. Jpn.* **65**, 2764 (1996)
- [5] M. Arai et al., *Phys. Rev. B* **56**, R4305 (1997)

Cooperation ¹Max-Planck-Institute for Solid State Research, Stuttgart, Germany; ²Univ. of Surrey, Guildford, United Kingdom; ³BESSY, Berlin, Germany; ⁴Univ. Paris-Sud, France

Non-existence of exact Kohn-Sham-equations in semi-relativistic current density functional theory

M. Taut, P. Machon, and H. Eschrig

One of the basic theorems for the widely used Kohn-Sham (KS) equations in density functional theory (DFT) is that for any *interacting* electron system in an external scalar potential $v^{ext}(\mathbf{r})$ there is a *non-interacting* model system, which provides the exact density $n(\mathbf{r})$ and energy E_{tot} of the ground state. This follows from the fact that the external potential is a unique functional of the density. If additionally a magnetic field (or vector potential $\mathbf{A}^{ext}(\mathbf{r})$) is involved, then semi-relativistic current density functional theory (CDFT) applies, but the external potentials $v^{ext}(\mathbf{r})$ and $\mathbf{A}^{ext}(\mathbf{r})$ are no more unique functionals of the densities $n(\mathbf{r})$ and $\mathbf{j}^p(\mathbf{r})$. Consequently, the existence of exact Kohn-Sham equations for the ground state cannot be proven. In standard CDFT implementations, the existence of exact KS equations is nevertheless presupposed. However, we have shown [1] using the exact analytical solutions of a two-electron quantum dot in a magnetic field [2] that in this system exact KS equations can exist only for certain orbital angular momenta. Consequently, the existence of exact KS equations is neither guaranteed for - nor restricted to ground states (see also Fig.), a result important for the application of KS theory to orbital magnetism.

[2] M. Taut, et al. Phys. Rev. A **80**, 022517 (2009)

[1] M. Taut, J. Phys. **A27**, 1045 (1994)

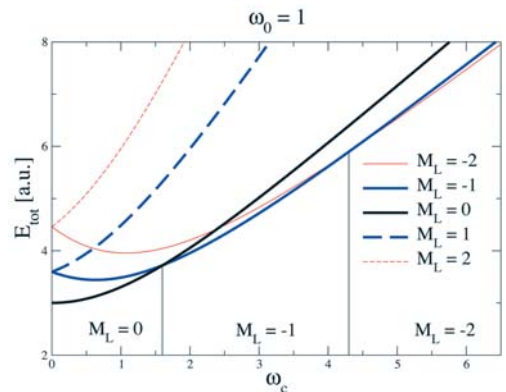


Fig.: Total energy of the harmonic two-electron quantum dot for fixed confinement frequency $\omega_0 = 1$ versus cyclotron frequency ω_c . The orbital angular momentum M_L is varied. Thick lines indicate states for which an exact Kohn-Sham system exists. The vertical lines indicate where the angular momentum of the ground state changes.

Electrodeposition of structured layers using defined magnetic field gradients

K. Tschulik, M. Uhlemann, J. Koza, K. Hennig, I. Mönch, V. Hoffmann, A. Gebert

Structuring of deposits has been demonstrated in ∇B -fields superimposed during the electrodeposition process in presence of paramagnetic ions as Cu^{2+} , Fe^{2+} or Co^{2+} . Defined ∇B -fields at disc-electrodes have been generated by a magnetic field template prepared from Fe wires ($\varnothing = 1$ mm, $l = 3$ mm) embedded in PVC (Fig. a) placed directly behind the electrode. The wire axes have been aligned perpendicularly to the horizontal electrode and magnetized by a homogeneous magnetic field B_{ex} of 0.5 T.

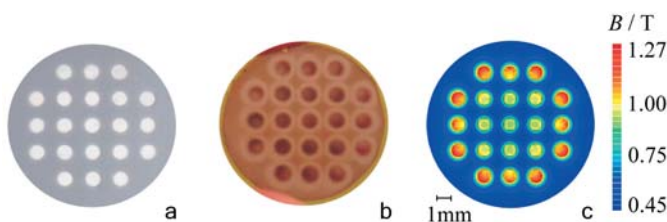


Fig.: Optical images of magnetic field template (a), structured Cu deposit (b), and simulated flux density distribution (c).

Obtained deposits show a direct correlation of the distribution of magnetic flux density B at the electrode and the morphology and thickness of the deposit. Maxima of deposit thickness correlate with maxima of $B\nabla B$, so evidently ∇B -fields can alter the current distribution at the electrode (Fig. b,c). As the depositions have been performed in the mass-controlled regime this observation indicates enhanced mass-transport of paramagnetic ions to these regions, leading to locally increased deposition rates. In contrast to that no structuring effect has been achieved for deposition of Bi from electrolytes containing diamagnetic Bi^{3+} ions. The structuring mechanism is mainly based on a sufficient influence of the field gradient force which attracts paramagnetic ions to regions of high field gradients. This force is overlapped by the Lorentzforce inducing a local MHD-convection.

Cooperation TU Dresden, Forschungszentrum Dresden-Rossendorf

Funded by DFG / SFB 609, Studienstiftung des deutschen Volkes

Highly ordered, half-metallic Co₂FeSi single crystals

C. G. F. Blum, S. Wurmehl, G. Friemel, C. Hess, G. Behr, B. Büchner, C. A. Jenkins¹, J. Barth¹, C. Felser¹, A. Reller², S. Riegg², S. G. Ebbinghaus³, T. Ellis⁴, P. J. Jacobs⁴, J. T. Kohlhepp⁴, and H. J. M. Swagten⁴

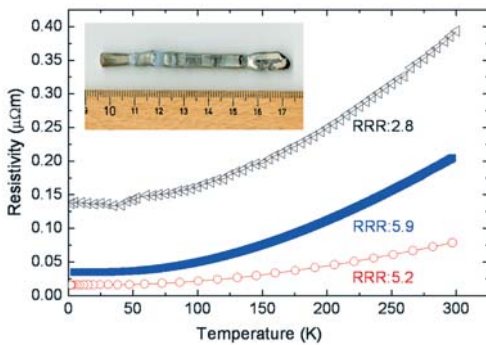


Fig.: Resistivity as a function of temperature for the Czochralski grown single crystal (triangles), the polycrystal (squares) and the zone molten single crystal (dots). The inset shows a rod obtained from the floating zone method containing large and high quality Co₂FeSi single crystals.

A wide variety of properties such as half-metallicity is found among Heusler compounds. In order to separate intrinsic and extrinsic properties, high quality single crystals are required. Here, we report on differently grown crystals (by arc-melting, floating zone and Czochralski method) of the half-metallic ferromagnet Co₂FeSi [1]. All crystals show excellent ordering, confirmed by Laue diffraction and nuclear magnetic resonance spectroscopy, resulting in outstanding electrical behaviour with low residual resistivity and high residual-resistivity-ratio. All Co₂FeSi crystals show a plateau in the resistivity below 50 K, which might point to half-metallic ferromagnetism. The cross-over from this unusual to more conventional transport (T^2 dependence) around 50 K indicates the onset of spin flip scattering and thus is indispensable for understanding the strong temperature dependence of Co₂FeSi tunnelling magnetoresistance-devices.

[1] C. G. F. Blum *et al.*, Appl. Phys. Lett. **95** (2009) 161903.

Cooperation ¹Johannes Gutenberg-Univ. Mainz, Germany; ²Univ. Augsburg, Germany; ³Martin-Luther-Univ. Halle-Wittenberg, Germany; ⁴Eindhoven Univ. of Technology, The Netherlands

Funded by DFG (Research Unit 559) and WU595/1-1.

Epitaxial thin SmCo₅ films with perpendicular anisotropy

M. Seifert, V. Neu, and L. Schultz

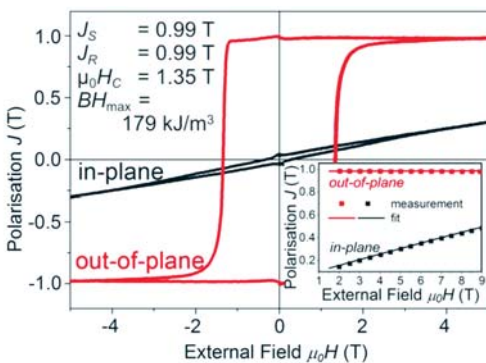


Fig.: Magnetic hysteresis of an epitaxial SmCo₅ film with perpendicular anisotropy. The flat and narrow hard axis loop can be fitted to a high uniaxial anisotropy with $K_u = 7.6 \text{ MJ/m}^3$.

SmCo₅ is the hard magnetic material with the highest uniaxial magnetic anisotropy and is long established for bulk permanent magnet applications. As a thin film, epitaxial SmCo₅ has only been realized on Cr buffered MgO(110) with a perfect in-plane texture, where the c-axis is oriented along the MgO[001] direction [1]. Due to the interest in materials with strong perpendicular anisotropy, recently several groups investigated polycrystalline Sm-Co based thin films on Cu templates with a preferred orientation of the c-axis perpendicular to the film plane [2]. In contrast to this, we achieved epitaxial growth of SmCo₅ with a perpendicular anisotropy without the use of an additional copper layer, and with a largely improved anisotropy constant of $K_u = 7.6 \text{ MJ/m}^3$ [3].

The films have been prepared by UHV pulsed laser deposition (PLD) at 700°C in on-axis geometry (KrF excimer laser, 248 nm, base pressure $< 5 \times 10^{-9}$ mbar) on a Ru buffered Al₂O₃(0001) substrate. SmCo₅ (10 $\bar{1}$ 1) pole figure measurements result in two sets of poles with 6-fold symmetry which are rotated 30° with respect to each other in agreement with two rotated variants of hexagonal SmCo₅ growing with the c-axis perpendicular to the surface. For film reduced thicknesses the intensity of one variant decreases, leading to a single orientation of SmCo₅ on Al₂O₃. The figure shows the highly anisotropic magnetic behavior of a 20 nm thin SmCo₅ film when measuring out of the film plane (i.e. parallel to the uniaxial anisotropy axis) and perpendicular to it, together with the extrinsic magnetic properties.

[1] A. Singh, *et al.*, J. Appl. Phys. **99**, 08E917 (2006)

[2] J. Sayama *et al.* Appl. Phys. Lett. **85**, 5640 (2004); S. Takei *et al.* J. Magn. Magn. Mater. **272**, 1703 (2004)

[3] M. Seifert *et al.*, Appl. Phys. Lett. **94**, 022501 (2009)

Huge tetragonal distortion in epitaxial films

J. Buschbeck, I. Opahle, M. Richter, U. K. Rößler, L. Schultz, S. Fähler

Strained coherent film growth is commonly either limited to ultrathin films or low strains. Here, we present an approach to achieve high strains in thicker films, by using materials with inherent structural instabilities. As an example, 50 nm thick epitaxial films of the $\text{Fe}_{70}\text{Pd}_{30}$ magnetic shape memory alloy are examined. Strained coherent growth on various substrates allows us to adjust the tetragonal distortion from $c/a_{\text{bct}} = 1.09$ to 1.39, covering most of the Bain transformation path from *fcc* to *bcc* crystal structure.

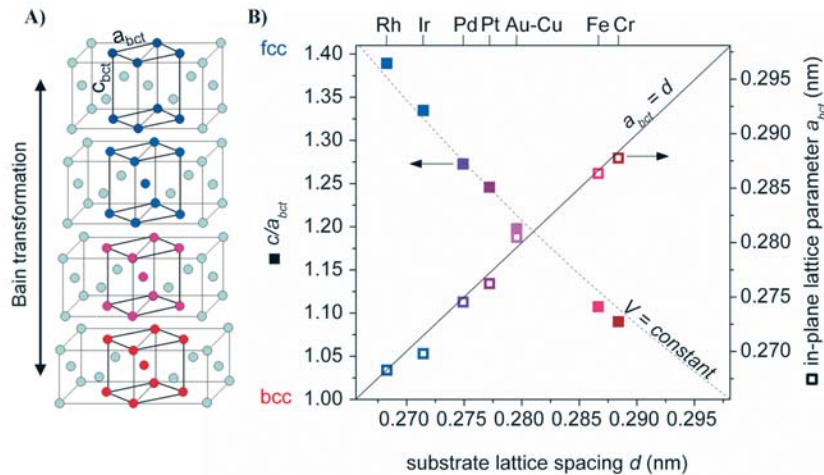


Fig.: A) Sketch of the Bain transformation between *fcc* (top) and *bcc* structure (bottom); B) c/a ratio (left scale) and in-plane lattice constants (right scale) of the Fe-Pd *bct* unit cell in dependence of the lattice spacings of the various buffer layers used (marked on top).

The magnetic properties of these films display considerable changes: The Curie temperature is increased more than 25% with respect to the value for $\text{Fe}_{70}\text{Pd}_{30}$ with *fcc* structure. This is accompanied by an increase of the magnetic anisotropy from near zero to values close to those of "fcc" bulk $\text{Fe}_{70}\text{Pd}_{30}$.

Softening of the crystal lattice and a flat energy landscape along the Bain path are not a unique feature of this alloy. Similar lattice instabilities may be exploited in various functional materials including (magnetic) shape memory, ferroelectric, multiferroic, or magnetocaloric materials for extended adjustability of their crystal structure in strained epitaxial films.

Cooperation Univ. Frankfurt; Johannes Gutenberg-Univ. Mainz

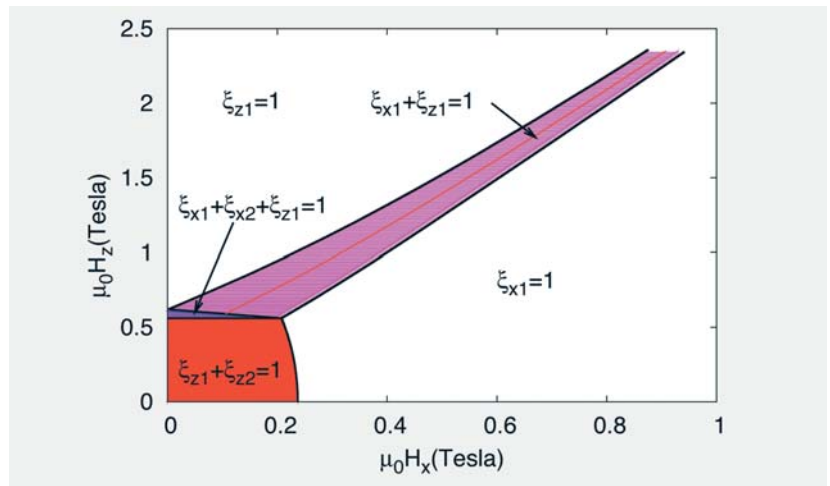
Funded by DFG via SPP1239 (www.MagneticShape.de)

Domain models for ferromagnetic shape memory materials

A. T. Onisan, A. N. Bogdanov, U. K. Rößler

The twinned martensitic microstructure of ferromagnetic shape-memory materials is transformed by modest applied magnetic fields. A domain model for the twin-variant and magnetic domain distribution in bulk systems of ferromagnetic shape-memory materials has been developed. The approach combines crystal elasticity, compatibility between twins with a (pseudo)-tetragonal lattice structure, and micromagnetic domain theory. The model has been applied to calculate detailed phase diagrams under external magnetic fields and stresses for the archetypical ferromagnetic shape-memory material Ni-Mn-Ga as a magnetic system with easy-axis anisotropy and for Fe-Pd with easy-plane fourfold anisotropies. The example shown is a phase diagram for Ni-Mn-Ga with two-variant microstructure composed of x - and z -variants. The phase diagrams allow to analyse the anhysteretic transformation and magnetization processes under combined

Fig.: Phase diagram for Ni-Mn-Ga under magnetic fields and compressive stress in z-direction in terms of volume fractions ξ of tetragonal x- and z-variants and internal magnetic domains 1 (2) with up (down) magnetization.



external magnetic fields and stresses. It is found that equilibrium domain and variant structures, caused by the depolarization, can own degrees of freedom in these systems that allow a rearrangement without energy cost.

Funded by DFG (SPP1239, A8)

Highly dispersive and low-energy spiral magnetic excitations in the frustrated chain compound Li_2CuO_2

S. L. Drechsler, W. E. A. Lorenz, R. Klingeler, N. Wizent, G. Behr, U. Nitzsche, J. Málek, B. Büchner

Li_2CuO_2 is the first and the most frequently studied compound of the growing class of frustrated edge-shared spin-chain cuprates. Owing to its structural simplicity with ideally planar CuO_2 chains it can be considered as a model quasi-one-dimensional (1D) frustrated quantum spin system. We performed various inelastic neutron scattering (INS) investigations of Li_2CuO_2 and detected the long sought quasi-1D magnetic excitations with a large dispersion along the CuO_2 -chains (Fig. 1). The total dispersion is governed by a surprisingly large ferromagnetic (FM) nearest-neighbor exchange integral $J_1 = -228$ K. An anomalous quartic dispersion near the zone center and a pronounced minimum corresponding to a low-energy spiral excitation over a commensurate collinear Néel ground state with a pitch angle of about 41° (Fig. 2) which points to the vicinity of a 3D FM-spiral critical point. The leading exchange couplings are obtained applying standard linear spin-wave theory. The 2nd neighbor inter-chain interaction suppresses a spiral state and drives the FM in-chain ordering below the Néel temperature. The obtained exchange parameters are in agreement with the exact diagonalization results for a realistic five-band extended HUBBARD Cu_3dO_2p model on $\text{Cu}_n\text{O}_{2n+2}$ clusters ($n = 2-6$) and with predictions derived from total energy calculations for various magnetic structures using the L(S)DA+U scheme, if a moderate value of the COULOMB repulsion on Cu-sites $U = 5.6$ eV is employed. The achieved detailed knowledge of the main exchange couplings derived from the INS-data provides a good starting point for an improved general theoretical description of other CuO_2 -chain systems.

[1] W.E.A. Lorenz et al., Europhysics Lett. **88**, 37002 (2009).

Cooperation R. Kuzian, Institute for Problems of Materials Science, Kiev, Ukraine; H. Rosner, Max Planck Institute for Chemical Physics of Solids, Dresden; A. Hiess, Institut Laue Langevin, Grenoble, France; M. Loewenhaupt, Institut für Festkörperphysik, TU Dresden

Funded by DFG, Emmy-Noether Gruppe

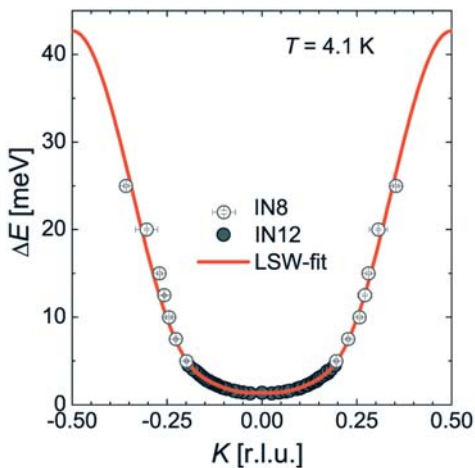


Fig. 1: The experimental magnon dispersion measured by various inelastic neutron scattering (INS) studies along the chain direction as compared with a linear spin wave (LSW)-fit.

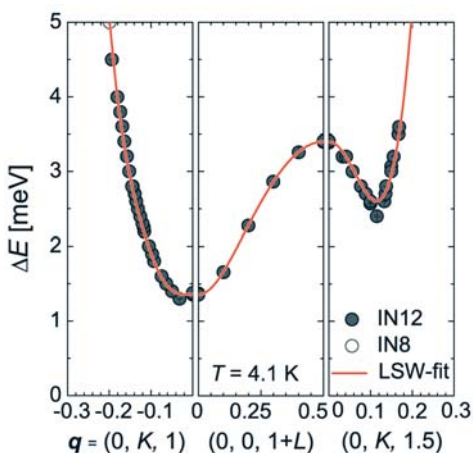


Fig. 2: The same as in Fig. 1 as measured by cold neutrons including also a direction perpendicular to the CuO_2 -chains (central panel). For the low-energy minimum corresponding to incommensurate spiral excitations see right panel.

Permanent Magnets

O. Gutfleisch, T. G. Woodcock, J. Thielsch, K. Güth, J. Lyubina, L. Römhildt,
K. Skokov, R. Schäfer, K.-H. Müller, L. Schultz

New energy concepts are required for the future of our industrial society resulting in e.g. an ever increasing emphasis on improving the efficiency of electricity transmission and utilisation and in the progressive replacement of oil-based fuels in transportation by electric motors. Recently, there is a much revived interest in various types of high performance permanent magnets (RPMs) based on rare earth intermetallic compounds. This is triggered by e.g. the growing demand for energy efficient technologies in which magnets often play a pivotal part. One prominent example is found in automobiles, specifically for traction motors in hybrid electric vehicles (HEVs). In this context, advanced permanent magnets are being studied in our group in terms of their fundamentals, processing and applications. This includes the determination of intrinsic magnetic properties, investigation of high pulsed magnetic field-induced phase transitions, detailed microstructural and micromagnetic analysis as well as the development of novel processing routes.



Fig. 1: Highest resolution TEM image of the $\text{Nd}_2\text{Fe}_{14}\text{B}$ phase in a Dy-free sintered magnet with the c-axis perpendicular to the imaging plane.

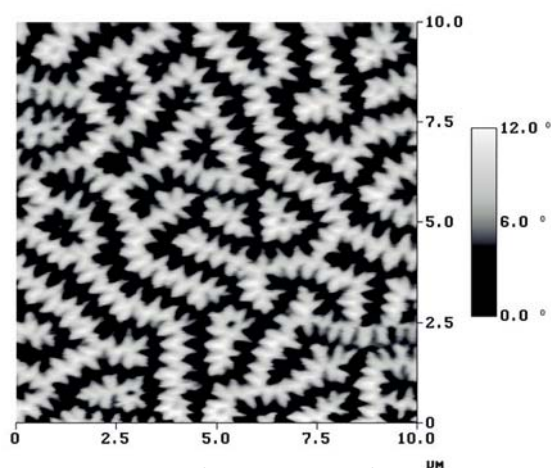


Fig. 2: MFM image of NdFeB $5\ \mu\text{m}$ thick film deposited by triode sputtering (cooperation Institute Néel Grenoble).

Generally, the major driver for research and development of RPMs is the need for maximised energy densities at various operating temperatures. This includes $\text{Pr}_2\text{Fe}_{14}\text{B}$ -type magnets for applications at 77 K together with high T_c superconductors, $\text{Nd}_2\text{Fe}_{14}\text{B}$ -type magnets with reduced Dy content and much improved temperature stability for electromotor applications at around 450 K, and a new generation of SmCo 2:17-type magnets for applications exceeding 670 K. It also includes magnetic microelectromechanical systems (mag-MEMS) for e.g. high speed permanent magnetic generators which require highly textured thick RPM films.

The characterisation and engineering of internal interfaces on a (sub-)nano scale is aimed at improved temperature stability of the magnet for HEVs applications.

Cooperation CNRS Grenoble, France; Toyota Motor Corporation, Japan; Tohoku Univ. Sendai, Japan; Univ. of Texas, USA; Vacuumschmelze Hanau, Germany; National Institute of Materials Science, Tsukuba, Japan

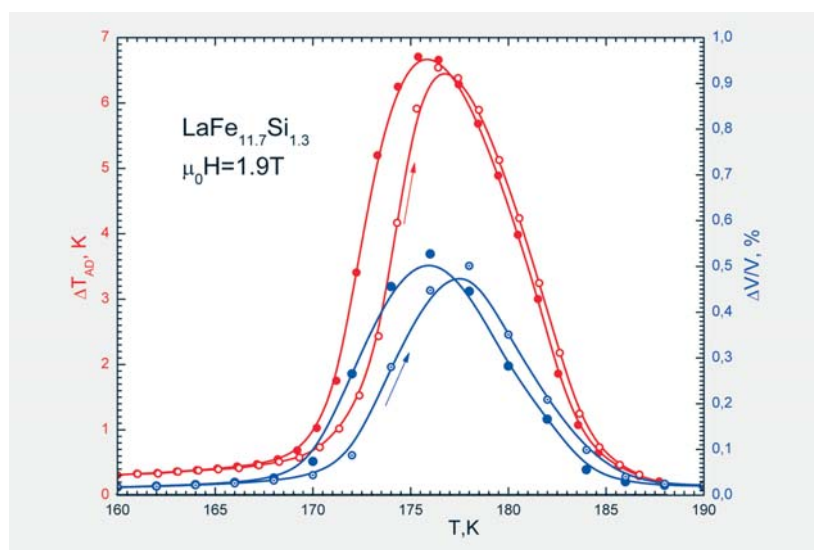
Funded by Toyota, Hans L. Merkle Stiftung, Bosch, Aichi-Steel, Forschungsvereinigung Antriebstechnik (FVA)

Magnetocaloric Materials

O. Gutfleisch, K. Skokov, J. Lyubina, M. Krautz, N. Scheerbaum, J. Liu, M. Richter

Magnetic refrigeration offers a solid state alternative to standard gas compression-based cooling that would simultaneously eliminate the need for harmful refrigerant gases and reduce energy requirements and hence carbon dioxide emissions. About ten years have passed since the discovery of the giant magnetocaloric effect in $Gd_5(Si,Ge)_4$, the magnetic refrigerant that re-ignited interest in magnetic cooling around room temperature. Since then a number of alternative magnetic refrigerants have emerged, resulting in a field that is yielding fundamental discoveries regarding solid-solid phase transitions whilst opening the way to new applications in cooling and other magneto-thermal and magneto-mechanical areas.

Fig.: An example for a solid-solid phase transition in $La(Fe,Si)_{13}$ correlating the resulting adiabatic temperature change with a strong magnetovolume effect, both in an applied magnetic field of 1.9 Tesla.



Our research focuses on the search for novel material systems, novel processing routes, and nano-architectures, the hysteresis properties, the time-dependency of magneto-structural and magnetoelastic transitions, the tailoring of operating temperature and of required magnetic fields, the engineering properties of magnetocaloric materials and ultimately the design of magnetic cooling devices. Systems of interest are the La-series alloy compounds, some transition-metal-based compounds, especially MnFePGe, as well as Heusler alloys.

Cooperation Imperial College London, UK; Vacuumschmelze Hanau, Germany; Istituto Nazionale di Ricerca Metrologica Torino, Italy; Univ. de Barcelona, Spain; Ames National Labs, USA; Univ. de Zaragoza, Spain; Camfridge Ltd., UK

Funded by EU (Solid State Energy Efficient Cooling - SSEEC), BASF Future Business

Research Area 3

Molecular nanostructures and molecular solids

Engineering of the energy level alignment at organic semiconductor interfaces by intramolecular degrees of freedom: transition metal phthalocyanines

M. Grobosch, V. Yu. Aristov, O. V. Molodtsova, C. Schmidt, and M. Knupfer

We have determined the energy level alignment at interfaces between various transition metal phthalocyanines (MnPc, FePc, CoPc, NiPc, CuPc) and gold using photoemission spectroscopy. Our results demonstrate that the transition metal center has a strong influence on the electronic properties of the phthalocyanine films as well as their interfaces with gold. This offers a route to adjust the hole injection barrier via the choice of otherwise equivalent molecular organic semiconductors. In particular, the interfaces MnPc/Au and CoPc/Au are characterized by a small hole injection barrier, which would be advantageous for applications. These are directly related to the presence of metal $3d$ states closest to the chemical potential. The nature of the molecular orbitals (metal $3d$ or ligandlike), that form the states closest to the chemical potential differ between MnPc and CoPc. In CoPc they are of predominantly metallic $3d$ character with a_{1g} symmetry and do not hybridize with the ligand π -system. Therefore, they are most likely to be highly localized due to the very small overlap between these orbitals of adjacent molecules and thus do not contribute to charge transport. Oppositely, the relevant states in MnPc strongly hybridize with the ligand, and thus, injection into these states with a small barrier from gold should also result in continuous charge transport across the interface. For details see: M. Grobosch *et al.*, *J. Phys. Chem. C* **113**, 13219 (2009).

Cooperation Institute of Solid State Physics, Russian Academy of Sciences;
TASC-INFM Laboratory; Univ. of Johannesburg
Funded by DFG, RFBR

Time-delayed release of the cytostatic carboplatin from multiwalled carbon nanotubes

D. Haase, M. Arlt, K. Krämer, A. Leonhardt, S. Oswald, M. Ritschel, R. Klingeler, S. Hampel, B. Büchner

The ongoing progress in developing tailored nanoscaled materials opens novel perspectives in applying nanotechnological approaches for medical therapy. Here, we show the feasibility of carbon nanotubes (CNT) as casing and carrier for cytostatics and demonstrate time-delayed release which is preferable in actual chemotherapies.

CNT/Carboplatin-hybrids have been synthesized via a liquid phase method using different types of CNT (multiwalled CNT with tubular and with herringbone structure, respectively). The relevant difference between the starting materials concerns their inner diameter which amounts 10–20 nm for the tubular CNT and about 100 nm for the herringbone type CNT. Interestingly, the carboplatin filling content is the same for both types, i.e. around 0.13 mg Pt per mg total mass. The release of the drug from the CNT was investigated by dispersion of the hybrids in cell culture medium and quantification of the drug present in the medium. Concerning the release, the tubular CNT/Carboplatin-hybrid was found to be favourable from which after 7 days 30 % of the Pt-content have been released, thereby demonstrating the carrier function for drugs. In comparison, the herringbone CNT/Carboplatin-hybrid released only 10 % of the Pt after 7 days.

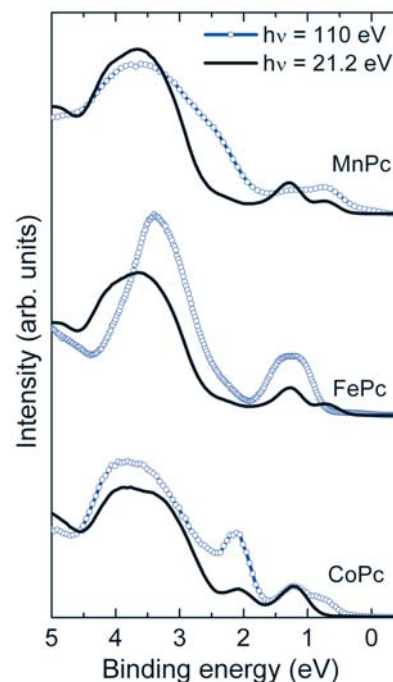


Fig.: Comparison of the valence band photoemission spectra of MnPc, FePc, and CoPc taken with photon energies of 21.2 and 110 eV (MnPc, CoPc) or 100 eV (FePc). Due to different cross sections, the data at 100/110 eV more strongly reflect metal $3d$ contributions.

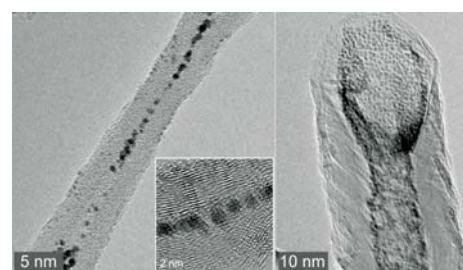


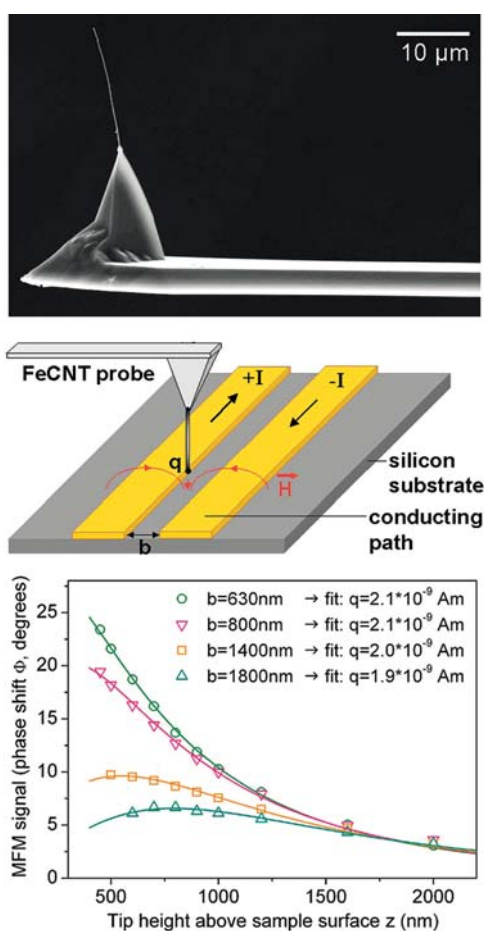
Fig. TEM images of two different types (tubular and herringbone) of CNT filled with Carboplatin.

Cytotoxicity of the hybrids as well as of the pure CNT was assessed *in vitro* using prostate carcinoma cells. CNT/Carboplatin-hybrids reduced cell viability with the same efficiency as pure Carboplatin at the same concentration. Carboplatin-loaded CNT effectively reduced colony formation of prostate cancer cell lines similar to Carboplatin solution. Our study highlights the potential of the use of CNT for biomedical applications.

Cooperation Department of Urology, TU Dresden University of Technology
Funded by DFG, EU

Iron filled carbon nanotubes – Novel high resolution high stability probes for quantitative magnetic force microscopy

F. Wolny, T. Mühl, U. Weissker, K. Lipert, A. Leonhardt, B. Büchner



Magnetic force microscopy (MFM) is a popular scanning probe technique to qualitatively image magnetic stray fields. To obtain quantitative information on the magnetic stray field or its gradients at the specimen's surface it is necessary to know the magnetic characteristics of the applied MFM tip. However, due to the complex geometry of conventional magnetically coated MFM probes, the effective magnetic tip coating involved in the tip-sample interaction depends on the geometry of the sample stray field. We use an iron filled carbon nanotube (FeCNT) which contains a long single-crystal iron cylinder of defined geometry (several microns in length, 10-50 nm in diameter) as MFM probe. This probe possesses well defined magnetic properties and thus permits a straightforward, universal calibration. The enclosed ferromagnetic wire can be regarded as an extended dipole of which only the monopole close to the sample surface plays a role during the imaging process. An easy calibration routine involving two parallel conducting paths that produce a defined magnetic field can be used to determine the probe's magnetic monopole moment needed for quantitative MFM measurements. Furthermore, the FeCNT probe has many more advantages over a conventional MFM probe: the mechanical and oxidation stability of the FeCNT leads to an extraordinarily long probe lifetime, the small diameter enables a high magnetic resolution and the magnetic shape anisotropy of the elongated iron cylinder ensures a stable direction of the probe magnetization.

Fig.: Top: Iron filled carbon nanotube attached to a conventional AFM cantilever. Middle: Setup for calibrating the FeCNT probe. The gold conducting paths of known geometry produce a defined magnetic field which is used to relate the MFM signal to actual magnetic field gradient values. Bottom: Calibration curves for a FeCNT probe. Conducting paths with different geometry (separation b between both paths) yield similar values of the corresponding probe magnetic monopole moment q .

Cooperation Ohio State Univ., USA
Funded by DFG

Space-charge-limited currents in organics with trap distributions

G. Paasch, S. Scheinert¹

Analytical approximations for space-charge-limited currents (SCLCs) in systems with exponential or Gaussian trap distributions were widely used in analyzing organic diodes. The current follows a power law with a transition into the trap-free SCLC at high voltages and an ohmic low voltage limit. The power coefficient γ is connected with either the decay constant or the variance of the distributions. Within these formulations, it is not possible to check the relevance of the numerous approximations needed to derive them. This concerns especially the relations of the contact work functions and of the layer

thickness with the trap concentration, the position of the center of the trap distribution and its maximum value. Application of the analytical approximations to results of full numerical simulations allows one to set limits for the parameter ranges in which the approximations can be applied. In the case of the exponential distribution the analytical approximation is rather good for high trap concentrations and thicker layers. However, the simulations reveal a number of additional peculiarities. Such, the high voltage limit is usually not the trap-free SCLC but ohmic and determined only by the anode barrier, the low voltage limit leads to a diodelike dependence with a large ideality factor and scaling with layer thickness and position of the trap distribution is extremely limited. In the case of the Gaussian trap distribution the simulations show indeed that the formula together with the connection between the power coefficient and the variance of the distribution fails completely. *Thus, in principle, earlier analyzes of experimental data should be revised by using numerical simulations.*

[1] G. Paasch and S. Scheinert, JOURNAL OF APPLIED PHYSICS **106**, 084502 (2009)

Cooperation ¹Institute of Solid State Electronics, Ilmenau Technical Univ.

Funded by DFG

Co Dimers on Hexagonal Carbon Rings Proposed as Subnanometer Magnetic Storage Bits

R. Xiao, D. Fritsch, M. D. Kuz'min, K. Koepernik, H. Eschrig, M. Richter, K. Vietze¹, G. Seifert¹

It is demonstrated by means of density functional and *ab initio* quantum chemical calculations [1], that transition-metal-carbon systems have the potential to enhance the presently available area density of magnetic recording by 3 orders of magnitude. As a model system, Co₂ benzene with a diameter of 0.5 nm is investigated. It shows a magnetic anisotropy of the order of 0.1 eV per molecule, large enough to store permanently one bit of information at temperatures considerably larger than 4 K. A similar performance can be expected, if cobalt dimers are deposited on graphene or on graphite.

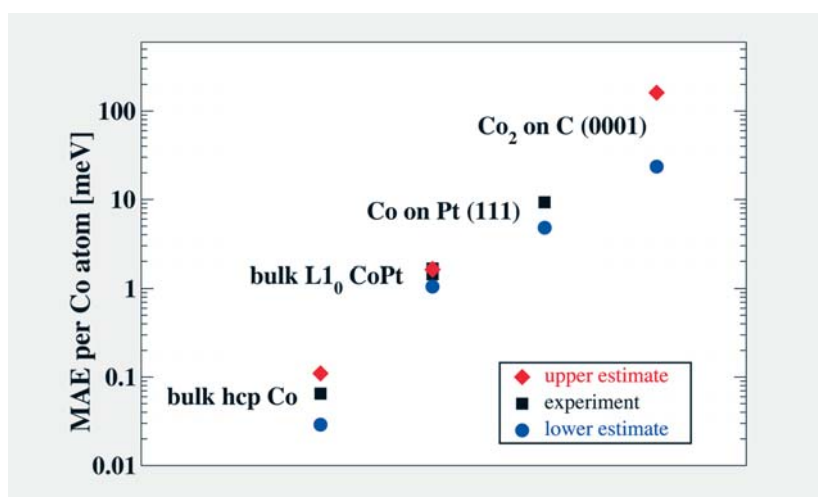


Fig. Magnetic anisotropy energy of Co atoms in different chemical and structural environments. Black squares denote experimental data, blue circles and red diamonds denote lower and upper estimate theoretical data. Bulk hcp Co, bulk L1₀ CoPt, Co atoms on the Pt (111) surface, and Co dimers on the graphite (0001) surface (our prediction) consecutively differ from each other by about 1 order of magnitude.

[1] R. Xiao et al. Phys. Rev. Lett. **103** (2009) 187201, selected for Virtual Journal of Nanoscale Science & Technology **20**, 2009.

Cooperation ¹TU Dresden

Funded by DFG, SPP 1145 and FOR 520.

The CVD synthesis of carbon coated magnetic nanoparticles

A. Leonhardt, V. Khavrus, E. M. M. Ibrahim, A. A. El-Gendy, S. Hampel, R. Klingeler, B. Büchner

Magnetic nanoparticles are receiving a lot of attention because this kind of heterostructure offers opportunities to develop devices and materials with new functions for different applications such as magnetic recording, tissue engineering, drug delivery/targeting, magnetic resonance imaging, magnetic bio-separation, and so on. The necessity of coating magnetic nanoparticles with protective shell like carbon is to achieve their stability against oxidation and corrosion and reduce their agglomeration.

Carbon coated Fe, Co and Ni nanoparticles (Fe@C, Co@C, and Ni@C, respectively) have been produced by high pressure chemical vapour deposition [1, 2]. The used method is based on the decomposition of a vapor consisting of metallocene ($\text{Me}(\text{C}_5\text{H}_5)_2$, Me = Fe, Co, or Ni) at a temperature in the range of 800–950 °C and a pressure of 10–30 bar in a horizontal steel reactor. A water-cooled finger is located in the cold zone of the reactor. The gas mixture is injected by using a nozzle-system. After the deposition process Me@C nanoparticles are concentrated on the cooled finger. Scanning and high resolution transmission electron microscopy images show that the nanoparticles have a size distribution from 2 to 100 nanometers and display the core/shell structure with one or more metal particles forming the core in a particular shell (see Fig.). The thickness of the protective carbon layers encapsulating the core particles amounts to 3–7 nm. The coated nanoparticles are ferromagnetic at least up to 400 K [1].

The proposed method can be extended for the synthesis various carbon coated alloys nanoparticles with different stoichiometric ratio of the core composition using different volatile metalorganic compounds.

[1] A.A. El-Gendy et al. Carbon 47 (2009) 2821–2828.

[2] V.O. Khavrus et al. J. Phys. Chem. C 2010, accepted.

Cooperation L.V. Pisarzhevsky Institute of Physical Chemistry, National Academy of Sciences of Ukraine, Kyiv, Ukraine; Sohag Univ. Egypt.

Funded by DFG, SMWK

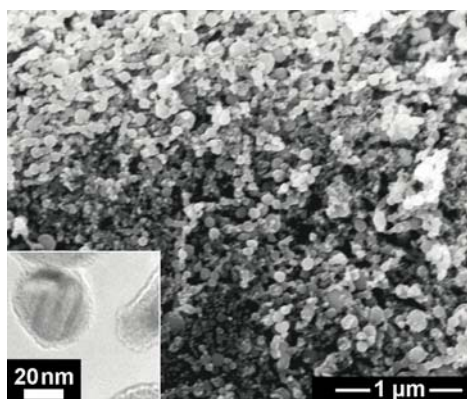


Fig.: SEM and TEM (inset) images of prepared Co@C nanoparticles.

Research Area 4

Metastable alloys

Liquid-liquid phase separation in binary Ti-Gd and Zr-Gd melts

W. Löser, S. Schmitz, H.-G. Lindenkreuz, N. Mattern, B. Schwarz, B. Büchner

Phase separated metallic glasses, as a new class of cluster materials, can be produced from complex alloys involving binary terminal systems with both negative and positive heats of mixing, respectively. It was shown that phase separation of the supercooled liquid state into two different glasses occurred in melt spun Zr-based metallic glass alloys due to the positive heat of mixing in the liquid state for Zr-R, where R is a Rare Earth element. Liquid phase separation below a critical temperature T_c can principally occur within either a stable or a metastable miscibility gap. While the former is an equilibrium phase diagram feature, the latter one lies beneath the liquidus curve ($T_c < T_L$). For thermodynamic modeling of glass forming systems experimental data are an urgent need. Liquid phase separation in two binary melt systems, Gd-Zr and Gd-Ti, related to phase separated metallic glasses are investigated by electromagnetic levitation experiments along with differential scanning calorimetric (DSC) studies. Gd-Ti samples quenched onto a copper chill substrate from temperatures below the binodal line exhibit typical coarse phase separated microstructures, assigning melt immiscibility. According to the undercooling experiments the miscibility gap of Gd-Ti melts extends at least from 10 to 80 at.% Gd (Fig.), much wider than reported previously [1]. The critical temperature is about 1580°C at Gd₂₀Ti₈₀. In the Gd-Zr system melt droplets quenched from the undercooled state exhibit concurrent coarse Gd and Zr primary phase constituents suggesting a metastable miscibility gap. The dissimilar phase separation features of the two binary systems investigated may imply different glass forming ability of the alloys.

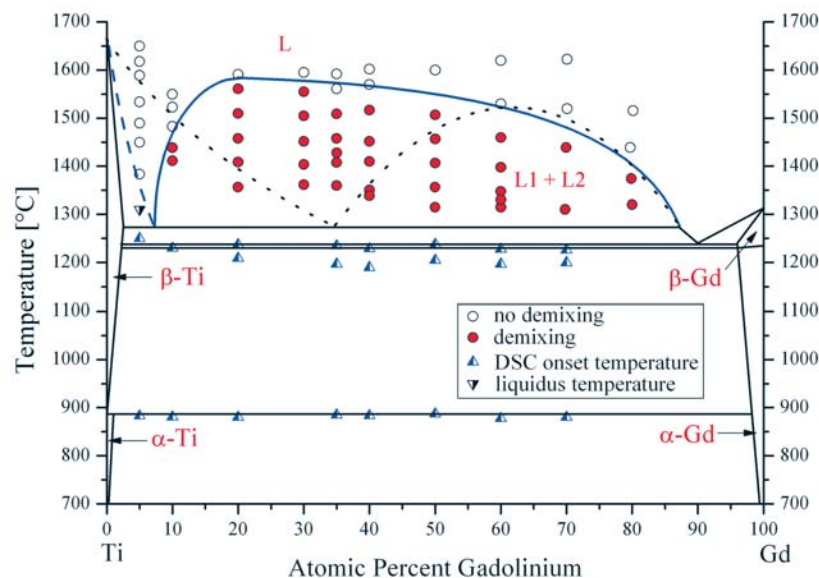


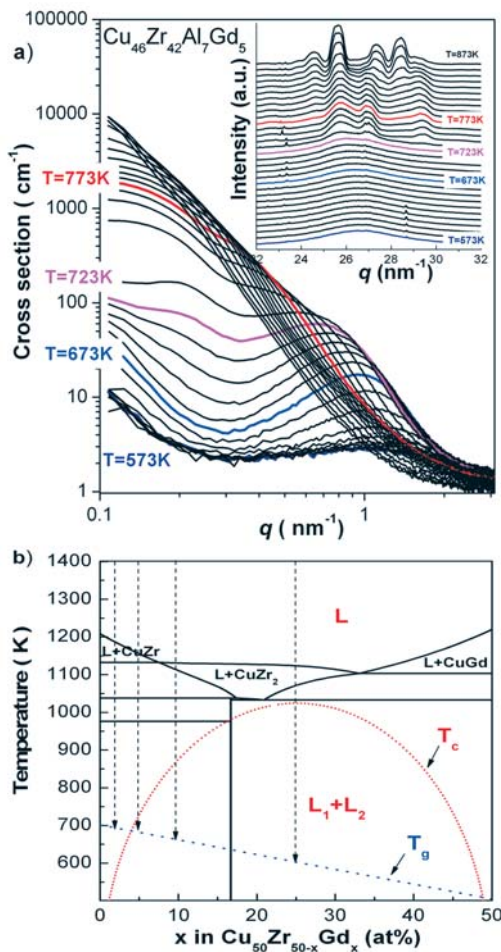
Fig.: Phase diagram of Gd-Ti with predicted liquidus and binodal line (dotted). Onset temperatures of the α -Ti to β -Ti solid state transformation, the eutectic/monotectic reaction and the liquidus temperature in case of Gd₅Ti₉₅ from the DSC measurements are denoted by triangles. Different microstructures of samples quenched from the various temperatures are denoted by open dots (macroscopically homogeneous microstructure) and filled dots (coarse phase separated microstructure), respectively. Full line: binodal line fitted from microstructure analyses. Dashed line: tentative liquidus line.

[1] J.L. Murray. In: T.B. Massalski, editor. *Binary alloy phase diagrams*, ASM International, Materials Park (OH); 2nd Ed., 1990, p.1935.

Cooperation DLR Cologne, TU Bergakademie Freiberg
Funded by Pakt für Forschung 2008

Phase separation in $\text{Cu}_{46}\text{Zr}_{47-x}\text{Al}_7\text{Gd}_x$ metallic glasses

N. Mattern, J. M. Park, J. H. Han, J. Eckert



Phase separated metallic glasses can be prepared in the Cu-Zr-Gd system by rapid quenching the melt as a consequence of the large positive enthalpy of mixing between gadolinium and zirconium [1,2]. The influence of composition on phase separation and microstructure of $\text{Cu}_{46}\text{Zr}_{47-x}\text{Al}_7\text{Gd}_x$ glasses was studied by in-situ synchrotron small-angle scattering (SAXS) combined with simultaneous measurement of wide angle X-ray scattering (WAXS). The question viewed is to which extend phase separation occurs in the glasses if the concentration of gadolinium is low, because for such compositions improved glass forming ability and plasticity is observed [1]. Low SAXS intensities of $\text{Cu}_{46}\text{Zr}_{47-x}\text{Al}_7\text{Gd}_x$ alloys with $x \leq 5$ indicate a homogeneous glass for the as-quenched state. Fig. 1a shows the in situ scattering data of the $\text{Cu}_{46}\text{Zr}_{42}\text{Al}_7\text{Gd}_5$ glass at elevated temperatures. The increase of the SAXS intensities between $T = 573\text{--}673\text{ K}$ give evidence of on-going phase separation by spinodal decomposition with a correlation length of about 6 nm prior to crystallisation as seen by WAXS at $T_x = 723\text{ K}$. For $x \geq 7$ at % the heterogeneities are already observed in the as-quenched glasses increasing in size for higher gadolinium contents. Fig. 1b shows the calculated pseudo-binary section along $\text{Cu}_{50}\text{Zr}_{50-x}\text{Gd}_x$ of the ternary phase diagram. The composition dependence of the miscibility gap of the under-cooled metastable liquid determines the structure formation of the glasses. Early stages of spinodal decomposition or an almost homogeneous glassy state is obtained if the critical temperature of liquid-liquid phase separation T_C is near to the glass transition temperature T_g . On the other side, if T_C is much larger than T_g , the microstructure becomes coarsened due to additional growth of the phase separated liquids during quenching.

Fig. 1a: SAXS and WAXS (inset) intensities of glassy $\text{Cu}_{46}\text{Zr}_{42}\text{Al}_7\text{Gd}_5$ at elevated temperatures. After measurement at $T = 573\text{ K}$ the temperature was stepwise increased by 10 K and repeated for each temperature.

Fig. 1b: Calculated pseudo binary section of the Cu-Zr-Gd phase diagram with the miscibility gap in the undercooled metastable liquid (red dotted line). The glass transition temperature T_g is extrapolated from the binary glasses (blue dashed line).

[1] E. S. Park et al. Scripta Mater. 57 (2007) 49.

[2] I.V. Stasi et al. J. Optoelectronics and Advanced Materials 10 (2008) 2963.

Cooperation Yonsei Univ. Seoul, Hasyllab at DESY Hamburg

Funded by DFG

In-situ AFM studies for corrosion analysis of Fe-based bulk metallic glasses

F. Gostin, A. Gebert, M. Uhlemann, U. Kühn, J. Eckert, L. Schultz

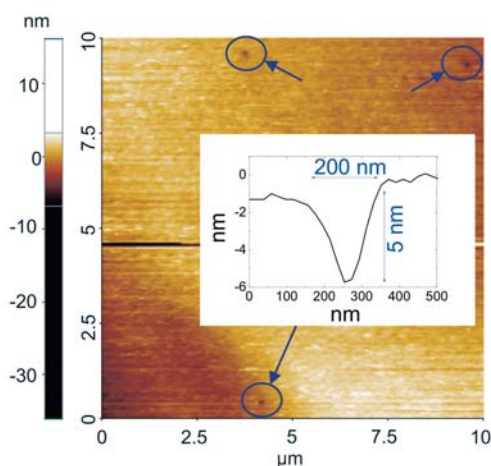


Fig.: In-situ AFM image of a corroding surface of a Fe-based BMG

In-situ atomic force microscopy (AFM) is a powerful technique which offers the possibility of direct observation of surface topographical changes during electrochemical measurements. An in-house built set-up allows a three electrode configuration to be used and full capability of control with an external potentiostat. Studies concerning the particularities of corrosion damage morphologies of Fe-based glassy alloys have not been performed up to now. Corrosion morphologies of classical crystalline alloys are strongly dependent on their structural characteristics such as grain boundaries, secondary phases, different orientation of grains etc. However, glassy alloys are missing most of these. In consequence, initiation of corrosion on such alloys is expected to be stochastic in nature. In-situ AFM realizes the detection of very early corrosion morphology features due to two factors: one is the very good depth resolution and the

second is the advantage of monitoring the same area of the surface throughout the corrosion process. This in turn allows tracing back the features from the late stages where they are easily visible. The figure shows an in-situ AFM image of a bulk glassy $(\text{Fe}_{44.3}\text{Cr}_5\text{Co}_5\text{Mo}_{12.8}\text{Mn}_{11.2}\text{C}_{15.8}\text{B}_{5.9})_{98.5}\text{Y}_{1.5}$ alloy surface taken after 1 hour in 0.5 M H_2SO_4 under free corrosion conditions. The arrows indicate initial centres of dissolution on the nano-scale otherwise not observable by optical or electron microscopy. Their appearance can be correlated with the chemical short range order of the glassy state.

Cooperation TU Dresden, Univ. Politehnica Bucarest

Geometrical aspects of the glass-forming ability of binary metallic alloys

V. Kokotin, A. Elsner, H. Hermann

The glass forming ability of metallic alloys and the stability of bulk metallic glasses have been addressed in numerous publications. Experimental rules have been established summarizing the experimental knowledge of conditions required for good glass forming ability. The atomic size distribution is one of the important variables controlling the stability of non-crystalline states. It is obvious that in dense-packed systems the local symmetry of clusters of atoms and the character of the medium-range order are correlated. If, e.g., the local clusters have essentially five-fold symmetry the system which the clusters are embedded in can not be periodic with respect to translational operations. We characterize a system of atoms given by the coordinates and the size of each atom in the following way: The Voronoi/Laguerre mosaic of the system is generated. A mosaic cell describes the cluster formed by the central atom and its neighbours. Two neighbouring clusters have one common interface. The number of edges of this interface is used as a measure for the symmetry of the rotation axis linking both clusters. For three-, four- and six-fold symmetry (approximated by the edge number) the link between the clusters would favour crystalline arrangements. For all other edge numbers the link would promote non-crystalline medium-range order. The complete system of atoms is now described by the number, f_{nc} , of all cluster interfaces with 5, 7, ..., edges divided by the number of interfaces with 3, 4, or 6 edges. The figure shows the result for dense-packed binary systems. Parameter f_{nc} is plotted versus size ratio and composition. Clearly, there is a confined region where f_{nc} is comparatively high. This is the region where geometrical aspects contribute to preferred glass forming ability. The binary bulk metallic glasses known until now fit into this region. Probably, further alloys situated in the high f_{nc} region are waiting for their discovery as bulk metallic glasses.

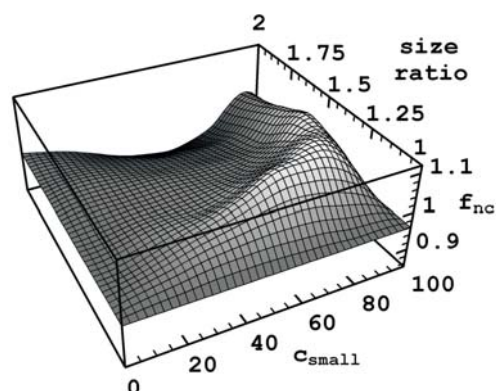


Fig.: Degree of non-crystalline local symmetry versus size ratio and fraction of small atoms for computer simulated dense packed binary mixtures of spherical atoms.

Cooperation Univ. of Appl. Sc. Darmstadt, Bergakademie Freiberg, RAN Novosibirsk
Funded by DFG

High-strength Al-based composites

S. Scudino, K. B. Surreddi, M. Sakaliyska, F. Ali, T. Gemming, U. Kühn, M. Stoica, N. Mattern, H. Ehrenberg, J. Eckert

As a result of the increasingly severe requirements for limiting fuel consumption and carbon dioxide emission, there is a growing trend to reduce the structural weight of vehicles in the transport sector. Among the advanced engineering materials for transport applications, Al-based metal matrix composites (MMCs) show the largest potential to reach this goal and to develop novel lightweight high-performance materials due to

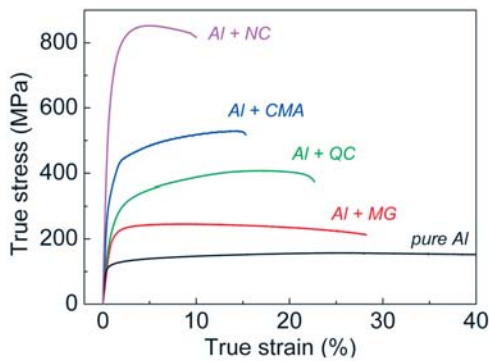


Fig.: Room temperature compression stress-strain curves for the Al-based metal matrix composites reinforced with different reinforcing particles: metallic glasses (MG), quasicrystals (QC) complex metallic alloys (CMA) and nanocrystals (NC).

their remarkable properties, including low density, high strength and good fatigue and wear resistance. In addition, MMCs offer the possibility to tailor their properties to meet specific requirements, which renders this type of materials quite unique in comparison to conventional unreinforced materials. In this project, several high-strength reinforcing phases, ranging from metallic glasses, complex metallic alloys and quasicrystals have been used to produce lightweight Al-based MMCs. The results indicate that the reinforcing particles are very effective for improving the mechanical properties of the metal matrix, revealing that the properties can be tuned within a wide range of strength and ductility as a function of size and volume fraction of the reinforcement.

Cooperation FZ Jülich; MPI Dresden; Univ. Frankfurt; Sejong Univ. Seoul/Korea; Univ. Torino, Italy; CNRS Grenoble, France; Slovak Univ. of Technology, Trnava, Slovak Republic

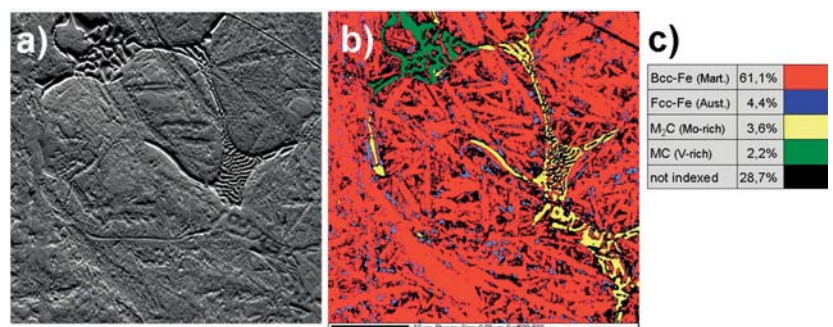
Funded by EU (NoE CMA), DAAD, BMBF, Pieas

High-strength martensitic Fe-base alloys

H. Wendrock, U. Kühn, H. Turnow, J. Stange, J. Hufenbach, C. Powik, U. Siegel, M. Kaiser, N. Mattern, H. Klauß, A. Güth, S. Roth, J. Eckert

Alloys of the type $\text{Fe}_{84.3}\text{Cr}_{4.3}\text{Mo}_{4.6}\text{V}_{2.2}\text{C}_{4.6}$ show outstanding mechanical properties when prepared by arc or induction melting under high purity conditions and cast into copper moulds. Compressive strength values of more than 4000 MPa combined with a compressive fracture strain of more than 20 % were achieved. Also tensile tests show large strength of about 1400 MPa already in the as-cast state of the material. A number of alloy variations with partial substitution of the carbide forming elements were investigated, and the mechanical properties of some promising compositions were studied at higher temperatures.

Fig.: a) SEM secondary electron micrograph showing a typical image of a specimen of $\text{Fe}_{84.3}\text{Cr}_{4.3}\text{Mo}_{4.6}\text{V}_{2.2}\text{C}_{4.6}$ polished for EBSD, FOV is $40\ \mu\text{m}$; b) coloured EBSD+EDS map at the same location on a grid of 500×500 points with 80 nm distance showing 4 phases (black = not recognizable, grain/phase boundaries or zones of very high deformation); c) colour legend of b) and numerical results of phase fractions



The complex microstructure (martensite, different complex carbides, residual austenite, see Fig. 1a for the initial alloy) was studied after appropriate metallographic preparation by highly resolved EBSD measurements combined with fast EDX mapping (Fig. 1b). The phase fractions and the typical grain size and shape could be determined in this way. Two main carbide types (MC and M_2C) were found forming a skeleton of lamellar primary carbides 0.2 to $1.5\ \mu\text{m}$ thick. Austenite regions are nearly equiaxed with a size of 0.3 to $1\ \mu\text{m}$, situated mostly between the martensite needles.

Tensile tests in-situ in the SEM showed that the fracture surface is highly connected with the interface between the carbides and the martensitic matrix. Thus, confinement of the primary carbide network is expected to be advantageous for increasing the tensile strength of this material.

Cooperation TU BA Freiberg, MPI for Iron research Düsseldorf

Hybrid cathodes of LiMPO_4 ($M = \text{Mn, Fe, Co, Ni}$) and carbon nanofilaments (CNF) for Li-ion batteries

H. Ehrenberg, A. Sarapulova, D. Mikhailova, N. N. Bramnik, J. Eckert

Phosphoolivines LiMPO_4 are promising cathode materials, but suffer from a low electronic conductivity and, depending on the specific 3d-transition metal M , pronounced instabilities in the charged state. For $M = \text{Fe}$ the fully charged state is very stable, and appropriate composite concepts, based on carbon coatings are well established with excellent performance but a rather low cell voltage of about 3.4 V. A much higher energy density would be possible for LiCoPO_4 , which offers cell voltages of about 4.9 V, but with a different working mechanism [1]. The charged state Li_xCoPO_4 is intrinsically unstable at elevated temperatures and suffers from oxygen release, especially in the presence of fine carbon particles [3]. To overcome limitations from low electronic conductivity and oxygen release in the charged state we have proposed a hybrid concept, based on an ordered array of carbon nanofilaments (CNF), which is in contact with a graphite current collector and coated with the electrochemically active phosphoolivines. Different processes have been established for the coating of the CNFs, e.g. for $M = \text{Fe}$ [4] or Mn [5]. Most promising results are obtained for $M = \text{Co}$ by the so-called triethylphosphite method, which allows a complete coverage of the CNFs with LiCoPO_4 , see the top figure for a single nanofibre and the bottom one for an ordered array of CNFs. The ongoing work is focused on building a demonstrator battery to determine the actual performance parameters for such hybrid cathodes in real devices.

[1] Bramnik et al. *Chem. Mater.* 19 (2007) 908-915.

[2] Ehrenberg et al. *Solid State Sciences* 11 (2009) 18-23.

[3] Bramnik et al. *Electrochem. Solid-State Lett.* 11 (2008) A89-A93

[4] Sivakumar et al. *J. Power Sources* 180 (2008) 553-560.

[5] Bramnik et al. *J. Alloys Compd.* 464 (2008) 259-264.

Cooperation Materials Science and Inorganic Chemistry at TU Darmstadt
Funded by DFG, SPP 1181 "NanoMat"

New Hydrides

O. Gutfleisch, C. Rongeat, I. Lindemann, C. Bonatto-Minella,
 R. Domènech Ferrer, C. Geipel, B. Gebel, M. Herrich, L. Dunsch,
 S. Oswald, M. Uhlemann, A. Gebert, L. Schultz

Human development has caused a depletion of natural energy resources and climate changes with non-predictable consequences. New energy concepts are required for the future of our industrial society. The only known energy carrier with a high energy density and no emission of greenhouse gas is hydrogen.

Research of solid-state storage of hydrogen – for e.g. zero-emission vehicle propulsion and other mobile applications – is pursued by exploring functional complex hydrides such as alanates and borohydrides. These materials offer several advantages over conventional metal hydrides provided thermodynamics, kinetics decomposition pathways and the reabsorption of hydrogen in modest conditions can be controlled and mastered. Our work includes the characterisation with high-pressure differential scanning calorimetry, gravimetric and pressure-composition-temperature analysis as well as the study of hydrogen dynamics using in-situ XPS, XRD and Raman in order to understand details of the complex sequence of transformations, to identify intermediate reaction products and rate determining steps in complex hydrides and reactive hydride composites.

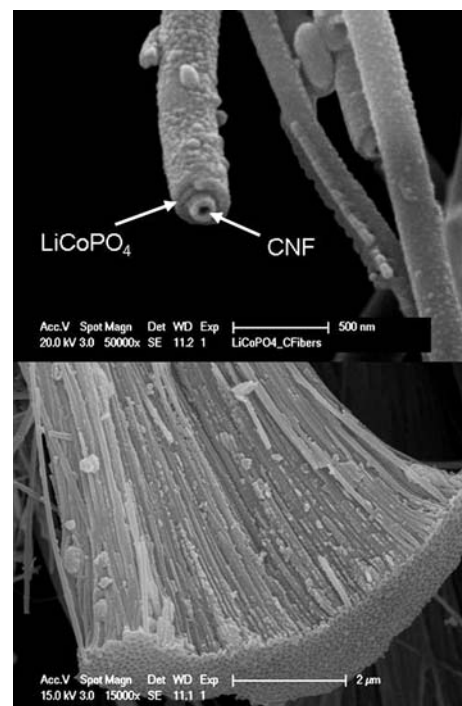


Fig.: (top) CNFs, coated with LiCoPO_4 by the triethylphosphite method, (bottom) an ordered array of CNFs, all coated with LiCoPO_4 .

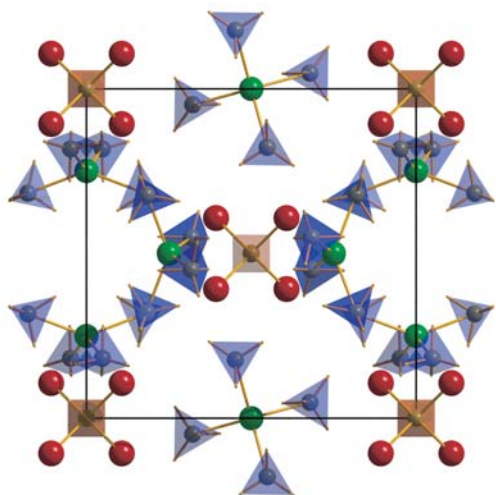


Fig.: Unit cell of $\text{Al}_3\text{Li}_4(\text{BH}_4)_{13}$. Four $(\text{BH}_4)^-$ tetrahedrons (blue) and one Al^{3+} cation (green) form the complex anion $[\text{Al}(\text{BH}_4)_4]^-$. Four Li^+ cations (red) bonded to one $(\text{BH}_4)^-$ tetrahedron (brown) in the centre form the complex cation $[\text{Li}_4(\text{BH}_4)]^{3+}$.

Novel processing techniques such as high hydrogen pressure reactive milling and high pressure annealing are used in order to identify new materials with high reversible hydrogen contents.

Recently we focused on the double-cation system Li-Al-borohydride, which shows a desorption temperature suitable for applications ($\sim 70^\circ\text{C}$) combined with a high gravimetric (17.2 wt.%) as well as volumetric (117 kg/m^3) hydrogen density. The material was synthesised via high energy ball milling of AlCl_3 and LiBH_4 in different molar ratios to find the adequate stoichiometry of the metathesis reaction. The structure of the compound was determined from high-resolution synchrotron powder diffraction and shows a unique complex structure within the borohydrides with the chemical formula $\text{Li}_4(\text{BH}_4)[\text{Al}(\text{BH}_4)_4]_3$. The compound forms a cubic unit cell containing a complex cation $[\text{Li}_4(\text{BH}_4)]^{3+}$ and a complex anion $[\text{Al}(\text{BH}_4)_4]^-$. Both are observed for the first time in solid state.

Cooperation EMPA, Switzerland; GKSS Research Centre Geesthacht, Germany; FZ Karlsruhe, Germany; Univ. of Amsterdam, Netherlands; Univ. of Geneva, Switzerland; Swiss-Norwegian Beam Line at ESRF, France; Univ. of Utrecht, Netherlands; Interdisciplinary Nanoscience Center, Univ. of Aarhus, Denmark

Funded by EU (NESSHY, COSY), HGF (FuncHy), ECEMP (Sächsische Exzellenzinitiative)

Research Area 5

Stress-driven architectures and phenomena

Spectral tunability of rolled-up microtube resonators on glass

V. A. Bolaños Quiñones, G. S. Huang, J. D. Plumhof, S. Kiravittaya, A. Rastelli, Y. F. Mei, and O. G. Schmidt

Microtubular resonators fabricated by the release and roll-up of strained nanomembranes guide light along the tube wall in the azimuthal direction. After a few rotations performed by the pre-stressed nanomembranes, the wall thickness of the final tube is smaller than the resonant wavelengths (or modes) supported by the resonator. As a consequence, the evanescent field of the resonant modes interacts with the media surrounding the microresonator, suggesting potential applications for on-chip components like filters and sensors. In order to fine tune the resonant modes, stepwise one-by-one monolayer (ML) Al_2O_3 coating on a SiO/SiO_2 rolled-up microtube with atomic layer deposition is carried out. As shown in Fig. 1a, rolled-up microtubes are fabricated on a transparent glass substrate, and their scanning electron microscopy (SEM) image is presented in Fig. 1b. By ALD coating, a controllable red shift of TM polarized resonant modes (labelled by solid circles and empty triangles in Fig. 1c) measured by photoluminescence (PL) is obtained over a wide spectral range. The measurements are well reproduced by finite-difference-time-domain (FDTD) simulations. In addition, a new group of resonant modes emerge when the Al_2O_3 coating is thicker than 200 ML (~ 20 nm). These modes are TE polarized (labelled by solid triangles) perpendicular to the previous group. Therefore, as the wall thickness increases, the diffraction loss of the TE modes decrease, allowing the microresonator to simultaneously support both TM and TE resonant modes. FDTD simulations reveal a progressive increase of the microtube refractive index after the consecutive Al_2O_3 coating, which cause a higher contrast between the microtube and the surrounding media resulting in the observed mode shifts.

Funded by Volkswagen Foundation (I/84 072) and a Multidisciplinary University Research Initiative (MURI) sponsored by the U.S. Air Force Office of Scientific Research (AFOSR) Grant No. FA9550-09-1-0550

Characterization of promising piezoelectric single crystals

A. Sotnikov, E. Smirnova, H. Schmidt, and M. Wehnacht

Hexagonal aluminum nitride (AlN) as a single crystal is of great interest due to its extreme physical and chemical properties. Attractive piezoelectric properties, very high values of sound velocity and the possibility to operate in harsh environment make AlN a very promising material for surface acoustic wave (SAW) applications. As expected, piezoelectric response in AlN can be observed up to very high temperatures.

Tetragonal LiAlO_2 crystal is attracting much attention as a promising substrate for growing III-nitrides like GaN/(Al,Ga)N which are technologically very important materials. Since LiAlO_2 shows high sound velocities and piezoelectric response, it might also be a potential candidate for SAW applications.

Material parameters including the elastic, piezoelectric and dielectric constants of AlN and LiAlO_2 piezoelectric single crystals, respectively, have been evaluated at room temperature by different methods: ultrasonic pulse-echo method, electromechanical resonance-antiresonance method and traditional dielectric method. Temperature dependences of the dielectric constant ϵ_{33} , the piezoelectric stress constant e_{33} as well as the elastic constants C_{33} and C_{44} of AlN have been measured at temperatures up to 500°C.

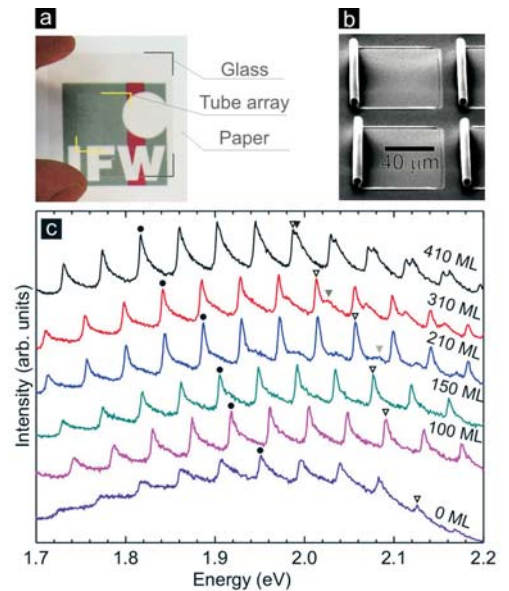


Fig.: (a) Rolled-up microtubular cavity array fabricated on a transparent glass substrate; (b) SEM image of microtubes rolled up from a square pattern. (c) Photoluminescence (PL) spectra of an ~ 7 μm diameter tube after coating with Al_2O_3 layers with increasing thicknesses (in MLs). Symbols mark the evolution of two TM modes (solid circles and empty triangles) and one TE mode (solid triangles).

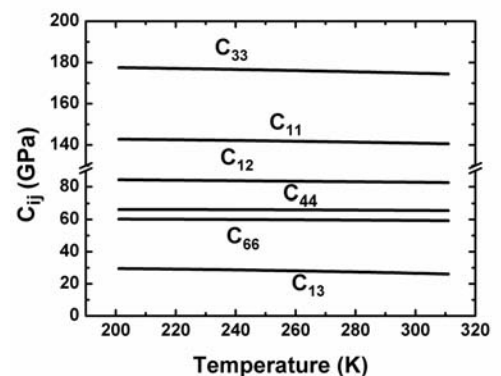


Fig.: Elastic constants of LiAlO_2 single crystal as a function of temperature.

The full set of the dielectric, elastic and piezoelectric constants for LiAlO_2 single crystal has been obtained in the temperature range from -70°C to $+50^\circ\text{C}$ for the first time (see Fig.). Using the experimental data, temperature coefficients of material parameters of LiAlO_2 have been calculated. The experimental results show that both materials, AlN and LiAlO_2 crystals are promising for surface- and bulk acoustic wave applications.

Cooperation Nitride Crystals Group, St. Petersburg, Russia; Tohoku University, Sendai, Japan.

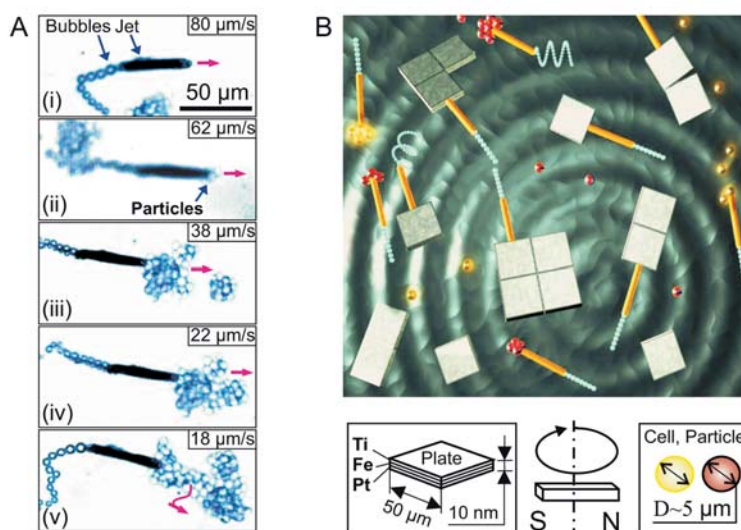
Funded by BMBF (InnoProfile), SMWK

Wireless Control of Tubular Catalytic Microbots for the Transportation, Assembly and Delivery of Microobjects

A. A. Solovev, S. Sanchez¹, Y. F. Mei, O. G. Schmidt

Recently significant attention has been dedicated towards the development of man-made synthetic catalytic micro- and nanomotors which can mimic biological counterparts in terms of propulsion power, motion control and speed. However, only few applications of such self-propelled vehicles have been described. Here we show wireless control of self-propelled catalytic Ti/Fe/Pt rolled-up microtubes (microbots). Magnetically directed movement of tubular microbots was accomplished through the incorporation of a ferromagnetic (Fe) layer. The extraordinary easy control over microbots movement by changing the direction of an external magnetic field during motion helps to specifically load and deliver cargo at the desired place. Microbots self-propel by ejecting microbubbles via platinum catalytic decomposition of hydrogen peroxide into oxygen and water. Furthermore, the physical characteristics of tubular microbots lead to high propulsion power achieving the absorption and delivering of up to sixty polymeric particles to a desired location as shown in Fig. 1A. As expected, their speeds slow down with more loaded particles. Our presented results are very promising for future drug delivery systems, biomedical applications require the use of biocompatible fuels for powering autonomous micromachines. Furthermore, one exciting direction could be a "microfactory" for nanoscience, which is illustrated in Fig. 1B. We are investigating on microbots powered by glucose fuels, their integration into Lab-On-a-Chip technologies, communication and self-organization.

Fig.: A) Transportation of polystyrene microparticles of $5\ \mu\text{m}$ diameter. A) Optical microscope images of microbot loading and transporting 3 (ii), 27 (iii), 44 (i) and 58 (iv) particles. Insets show microbot's average speeds. B) Schematic representation of "microfactory" where wireless control of microbots by an external magnet, assisted load, transport, delivery and assembly of microparticles and nanoplates in fuel solution.



Cooperation ¹National Institute for Materials Science, Tsukuba, Ibaraki, Japan; School of Physical & Mathematical Sciences, Nanyang Technological Univ., Singapore

Multiferroic Oxide Film Structures

K. Dörr, O. Bilani, K. Boldyreva, M. C. Dekker, C. Deneke, E. Wild, A. Herklotz, J.-W. Kim, K. Nenkov, A. Rastelli, A. D. Rata, O. G. Schmidt, L. Schultz

Multiferroic HoMnO_3 films of thicknesses $\leq 1 \mu\text{m}$ were prepared by pulsed laser deposition (PLD) and have been investigated by optical Second Harmonic Generation (SHG) [1] and SQUID magnetometry in order to reveal the ferroic phases present in the thin films (thesis of J.-W. Kim). While HoMnO_3 is a single-phase low-temperature multiferroic, magnetic films epitaxially grown on piezoelectric substrates of PMN-PT(001) ($\text{Pb}(\text{Mg}_{1/3}\text{Nb}_{2/3})_{0.72}\text{Ti}_{0.28}\text{O}_3$) provide a model system for strain-coupled two-phase multiferroics [2] comprising of a ferroelectric and a magnetic component. For the magnetic films, phase-separated manganites [3] and $\text{La}_{1-x}\text{Sr}_x\text{CoO}_3$ with a potentially strain-controllable spin state of the Co ions have been investigated. Cobaltite films reveal spin-state control by strain for $x = 0$ [4], and a tendency for defect formation resulting from spin-state-related enhanced thermal expansion. In User projects at the CNMS, ORNL the reversible strain induced in coherent superlattices of $[\text{La}_{0.7}\text{Sr}_{0.3}\text{MnO}_3/\text{SrTiO}_3]_n$ (Fig.) and in buffer layers of $\text{LaAl}_{1-x}\text{Sc}_x\text{O}_3$ offering an adjustable in-plane lattice parameter of $3.8 - 4 \text{ \AA}$ has been demonstrated using four-circle x-ray diffraction. Strain application in thin film membranes is promising through the approach of rolled-up epitaxial oxide layers.

The light emission from InGaAs quantum dots embedded in GaAs microring resonators has been efficiently tuned employing the reversible compressive or expansive strain from PMN-PT crystals at 10 K [5], indicating a promising potential of the strain tuning for establishing resonances which are required to achieve entangled photon states. Light-control of the metal or insulator state has been demonstrated for epitaxial electron-doped films of $\text{La}_{0.7}\text{Ce}_{0.3}\text{MnO}_3/\text{SrTiO}_3(001)$ [6].

[1] T. Kordel et al., Phys. Rev. B **80**, 045409 (2009)

[2] K. Dörr et al., Eur. J. Phys. B **71**, 361 (2009)

[3] M. C. Dekker et al., Phys. Rev. B **80**, 144402 (2009)

[4] A. Herklotz et al., Phys. Rev. B **79**, 092409 (2009)

[5] T. Zander et al., Optics Express **17**, 22452 (2009)

[6] E. Beyreuther et al., Phys. Rev. B **80**, 075106 (2009)

Cooperation TU Dresden, Univ. of Bonn, Oak Ridge National Laboratory, TN, USA

Funded by DFG, DAAD, IMPRS

Rolled-up Cr microtubes alignment in microfluidic systems by standing surface acoustic waves

X. H. Kong, H. Schmidt, C. Deneke, H. X. Ji, D. J. Thurmer, M. Bauer, S. Menzel, and O. G. Schmidt

Recently, surface acoustic waves (SAW) have been established as a promising approach for fast, reliable manipulation and alignment of micro- and nanostructures in microfluidic systems. Here, the alignment of rolled-up Cr microtubes dispersed in propylene carbonate solvent by standing surface acoustic waves (SSAW) is demonstrated. For our experiments, a pair of electrically optimized, opposing interdigital transducers (IDTs) is fabricated on top of a 128° rotated Y-cut LiNbO_3 substrate. Each IDT launches a SAW with a wavelength of $130 \mu\text{m}$ at a corresponding frequency of about 30 MHz, to form a SSAW pattern in the area of a fluidic channel between the substrate and a glass cover. For the alignment experiment, the capillary is filled with Cr tube suspension. In the start, the rolled-up microtubes are randomly dispersed in the fluidic channel (see Fig. inset). When two rf power signals (here: 6 dBm) are simultaneously applied to both IDT ports in equal portions, a standing wave pattern accompanied by an appropriate electric field

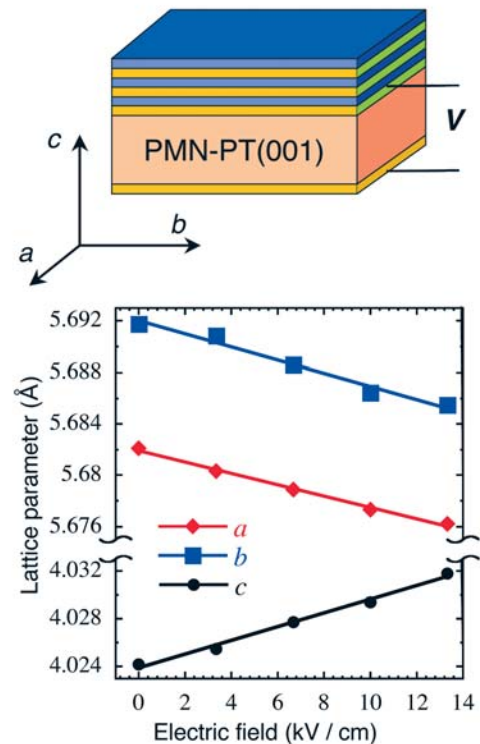


Fig.: Scheme of a reversibly strainable oxide superlattice on a piezoelectric substrate of PMN-PT (top) and electrically controlled lattice parameters of PMN-PT measured by x-ray diffraction (bottom).

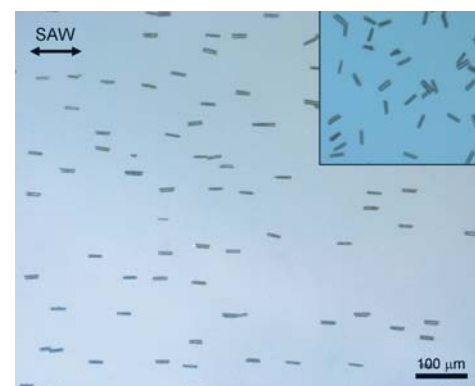


Fig.: Typical optical micrograph of Cr microtube alignment by standing surface acoustic waves on a LiNbO_3 substrate. The $30 \mu\text{m}$ long Cr microtubes are orderly aligned in parallel to the SAW propagation direction (denoted by the double arrows). The inset shows the initial random dispersion of the microtubes before starting of SAW excitation.

pattern forms in the capillary. Due to these patterns, the rolled-up Cr microtubes are aligned into one direction, with their axis parallel to the propagation direction of the SAWs. Such an aligned tube area is depicted in the figure. The proportion of microtube alignment by SSAWs at a certain frequency depends on the length of the tubes and the applied signal power. In a setup with two IDT pairs, arranged perpendicularly to each other, the alignment of the Cr microtubes can be switched by this method between the two main directions.

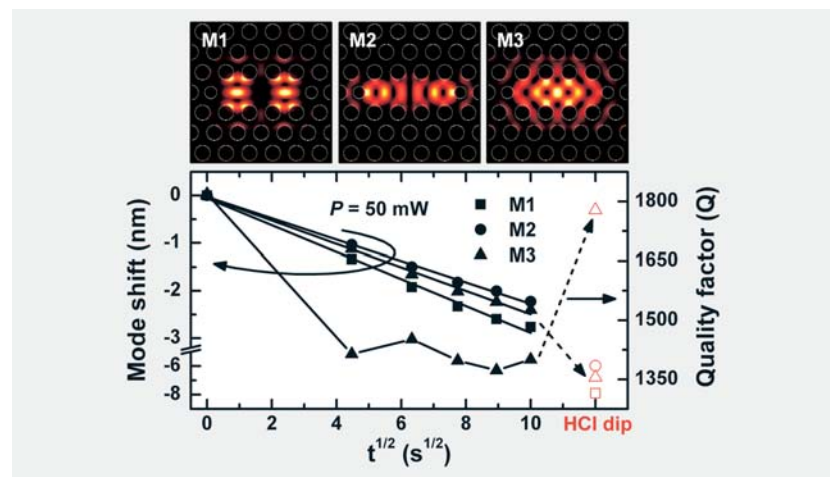
Funded by BMBF (InnoProfile)

Optical microcavity tuning by local laser processing

H. S. Lee, S. Kiravittaya, S. Kumar, J. D. Plumhof, A. Rastelli, O. G. Schmidt

Photonic crystal (PhC) optical microcavities are attracting much interest for their potential application in advanced optical devices such as switches, filters, multiplexers, low-threshold lasers, and cavity quantum electrodynamics. For such applications, it is necessary to control and tune the resonant wavelength of the PhC cavity modes. The PhC cavity resonances (or modes) can be tuned by adjusting the PhC lattice and defect geometries. However, the exact spectral position of the modes can not be predicted with the accuracy required for some applications, because the modes are highly sensitive to fabrication parameters. Therefore, postprocessing tuning techniques able to compensate for fabrication imperfections are particularly demanded. Most of tuning techniques presented so far either modify the properties of the whole sample, which prevents the local tuning of a single nanocavity, or need extra materials and processing tools.

Fig.: Top: FDTD-calculated electric field intensity profiles for the TE modes M1, M2, and M3 confined in a PhC nanocavity. Bottom: mode wavelength shift for three modes and quality factor for M3 as a function of the square root of the oxidation time at a laser power $P = 50$ mW. The open symbols indicate the values after a dip in HCl for 5s.



In this work, we investigated the local tuning of optical modes in GaAs PhC microcavities by continuous wave laser-assisted oxidation in air atmosphere. The oxide growth leads to controllable shifts of the cavity modes to shorter wavelengths. By irradiation with a focused laser beam at power levels of a few tens mW, PhC nanocavity modes blue-shift by up to 2.5 nm. The mode shifts, which are different for different modes of the same cavity, can be controlled by varying the irradiation conditions and are well explained by finite-element-method (FEM) and finite-difference time-domain (FDTD) simulations. [1] H. S. Lee et al. Appl. Phys. Lett. 95, 191109 (2009).

Cooperation EPFL Institute of Photonics and Quantum Electronics, Switzerland; Institute of Photonics and Nanotechnology, Italy; COBRA Research Institute, Netherlands

Funded by DFG (FOR 730), Korea Research Foundation (KRF-2008-357-C00035)